

Dear Dr Roche,

Thank you for your handling of our manuscript, and constructive comments. Please see response to your points below. We hope to have addressed your concerns, which may be due to poor communication on our part.

I have read in depth your manuscript, the concerns expressed by reviewer #2 and your response to reviewers.

I still find two aspects problematic:

1-/ Reviewer #2 highlighted that the RMSE metrics on which you base the ATAT tool needs to include for observational and downscaling uncertainties. Though you discuss at length in your response to reviewers the different sources of uncertainties and their origin, you did not reply to this specific request in positive or negative. I am sure the reviewer is well aware that structural uncertainty is present in any modeling work so this is not the point for discussion. You advocate for the user of your tool to have run ensemble experiments of their ice-sheet model which I understand, but how and where does these ensemble runs come into the uncertainty in your tool? Do you consider running your tool for each of the member independently and accounting for such uncertainty a posteriori? But how? I feel that the request of reviewer #2 in this context regarding equations 1&2 is a valid one, unless I miss part of the reasoning of course.

ATAT does include a procedure which accounts for observational and downscaling uncertainties, though this is not reflected in equations 1 and 2 alone. ATAT categorises the dated-locations using the criteria of modelled ice cover, agreement within dating (observational) error and those within margin uncertainty (downscaling uncertainty). By applying equations 1 and 2 to these categories of dates, observational and downscaling uncertainties can be accounted for. We have clarified this in the text (lines 469-473). Note that ATAT also outputs the percentage of dates in each category, so that models which do not agree with many sites can be identified (list at end of Figure 5).

We chose to retain these categories, rather than produce a single metric, so that a user may select the appropriate metric for their model experiment.

We advocate applying the tool to members of an ensemble (lines 487-490) so that members may be ranked or a weighting scheme applied when calibrating a model ensemble. An alternative is also suggested in the text, that ATAT be applied to a model with an independently derived uncertainty distribution of deglacial timing at each model cell. For example, an ensemble could be run producing a mean deglacial timing and a standard deviation of deglacial timing. The user could then use the extremes of this modelled uncertainty to test which dates agree within dating error and margin uncertainty (lines 491-494).

Perhaps some of this concern comes from the difference between our approach and that of Reviewer 2. As many of us come from a data-based background, we know that some uncertainties are poorly defined. In our case, all data collected relies upon stratigraphic interpretation. This is why we are keen to retain the discussion of data uncertainty (Section

2.1), and to air the possibilities of also using the model to identify data outliers (lines 495; 580-584; 596-597).

2-/ In the new paragraphs that have been implemented in your manuscript I read: "Structural uncertainty is related to parametric uncertainty, but has a broader remit, and is defined here as all uncertainty that arises within a model due to a lack of physical understanding of the system in question." pp line and following. Does this mean you have, for this particular manuscript, specific definition of structural uncertainty which is not the common one? Could you highlight the reason for doing so and what is the exact difference with the common definition?

Having read some more literature around structural uncertainty, we have refined the definition stated and added reference to the relevant literature. In geoscience it seems that structural uncertainty is that related to code structure, which processes are included and how. Confusion was introduced as other disciplines have a different definition. We have also noted a means for accounting for this uncertainty (though it is not commonly done in palaeo-ice sheet modelling), by conducting a multi-model comparison including models with different process formulations (lines 225-233).

ATAT 1.1, an Automated Timing Accordance Tool for comparing ice-sheet model output with geochronological data

Jeremy C. Ely¹, Chris D. Clark¹, David Small² and Richard C.A. Hindmarsh³

¹Department of Geography, The University of Sheffield, Sheffield, S10 2TN, UK

²Department of Geography, Durham University, Durham, DH1 3LE, UK

³British Antarctic Survey, High Cross, Madingley Road, Cambridge, CB3 0ET, UK

Correspondence to: Jeremy C. Ely (j.ely@sheffield.ac.uk)

Abstract. Earth's extant ice sheets are of great societal importance given their ongoing and potential future contributions to sea-level rise. Numerical models of ice sheets are designed to simulate ice sheet behaviour in response to climate changes, but to be improved require validation against observations. The direct observational record of extant ice sheets is limited to a few recent decades, but there is a large and growing body of geochronological evidence spanning millennia constraining the behaviour of palaeo-ice sheets. Hindcasts can be used to improve model formulations and study interactions between ice sheets, the climate system and landscape. However, ice-sheet modelling results have inherent quantitative errors stemming from parameter uncertainty and their internal dynamics, leading many modellers to perform ensemble simulations, while uncertainty in geochronological evidence necessitates expert interpretation. Quantitative tools are essential to examine which members of an ice-sheet model ensemble best fit the constraints provided by geochronological data. We present an Automated Timing Accordance Tool (ATAT version 1.1) used to quantify differences between model results and geochronological-data on the timing of ice sheet advance and/or retreat. To demonstrate its utility, we perform three simplified ice-sheet modelling experiments of the former British-Irish Ice Sheet. These illustrate how ATAT can be used to quantify model performance, either by using the discrete locations where the data originated together with dating constraints or by comparing model outputs with empirically-derived reconstructions that have used these data along with wider expert knowledge. The ATAT code is made available and can be used by ice-sheet modellers to quantify the goodness of fit of hindcasts. ATAT may also be useful for highlighting data inconsistent with glaciological principles or reconstructions that cannot be replicated by an ice sheet model.

1 Introduction

Numerical models have been developed which simulate ice sheets under a given climate forcing (e.g. Greve, 1995; Rutt et al., 2009; Pollard and DeConto, 2009; Winkelmann et al., 2011; Gudmundsson et al., 2012; Cornford et al., 2013; Pattyn, 2017). When driven by future climate scenarios, these models are used to forecast the fate of the Antarctic and Greenland ice sheets (e.g. Seddik et al., 2012; DeConto and Pollard, 2016), providing predictions of their potential contribution to future sea level rise. However, incomplete knowledge of ice physics, boundary conditions (e.g. basal topography) and parameterisations of physical processes (e.g. basal sliding, calving), as well as the difficulty of predicting future climate, lead to model-based uncertainty in these predictions (Applegate et al., 2012; Briggs et al., 2014; Ritz et al., 2015). Observations of ice marginal fluctuations (decades) and the processes of ice calving, flow or melting (subaerial or submarine) that facilitate or drive such variations, provide a powerful means to understand the processes leading to the possibility of deriving new formulations that improve

37 the realism of modelling. However, the short-time span (decades) of these observations limits their being used to
38 constrain, initialise or validate modelling experiments (Bamber and Aspinall, 2013). Conversely, palaeo-ice
39 sheets, especially from the last glaciation (~21,000 years ago), left behind evidence which provides the
40 opportunity to study ice sheet variations across timescales of centuries to millennia, albeit with increased
41 uncertainty in exact timing.

42 Numerous modelling studies have aimed to simulate the growth and decay of palaeo-ice sheets, producing
43 hindcasts of ice-sheet behaviour (e.g. Boulton and Hagdorn, 2006; Hubbard et al., 2009; Tarasov et al., 2012;
44 Gasson et al., 2016; Patton et al., 2016). Results from these hindcasts may be compared with empirical data
45 recording ice sheet activity, so as to discern which parameter combinations produce results that best replicate the
46 evidence of palaeo-ice sheet activity. Three classes of data are of particular use for constraining palaeo-ice sheets;
47 (i) geomorphological data, (ii) geophysical data, and (iii) geochronological data. Ideally, all three classes of data
48 should be used to quantify the goodness of fit of a hindcast.

49 Geomorphological evidence comprises the landforms created by the action of ice upon the landscape, and can
50 typically provide data on ice extent, recorded by moraines and other ice marginal landforms and on ice-flow
51 directions recorded by subglacial landforms such as drumlins. Such landforms can be used to decipher the pattern
52 of glaciation (e.g. Kleman et al., 2006; Clark et al., 2012; Hughes et al., 2014). Two tools, namely Automated
53 Proximity and Conformity Analysis (APCA) and Automated Flow Direction Analysis (AFDA), have already been
54 developed which can compare modelled ice margins (APCA) and flow directions (AFDA) to the
55 geomorphological evidence base (Napieralski et al., 2007).

56 Geophysical data, in the form of relative sea level measurements and present day uplift rates, provide information
57 regarding the mass-loading history of an ice sheet. Palaeo-ice-sheet model output is often evaluated against such
58 data by use of glacio-isostatic adjustment models (e.g. Tushingham and Peltier, 1992; Simpson et al., 2009;
59 Tarasov et al., 2012; Auriac et al., 2016).

60 Geochronological evidence attempts to ascertain the absolute timing of ice advance and retreat using dated
61 material (e.g. organic remains dated by radiocarbon measurement) found in sedimentary contexts interpreted as
62 indicating ice presence or absence nearby. It enables reconstruction of the chronology of palaeo-ice sheet growth
63 and decay (Small et al., 2017) and is the underpinning basis for empirically-based ice sheet margin reconstructions
64 (e.g. Dyke, 2004; Clark et al., 2012; Hughes et al., 2016). Although widely used in empirical reconstruction of
65 palaeo-ice sheets, geochronological data has rarely been directly compared with ice sheet model output (although
66 see Briggs and Tarasov, 2013). Such a comparison could be useful both for constraining ice-sheet model
67 uncertainty and for identifying problems with the geochronological record. For example, a poor fit between model
68 output and empirical data on timing could inform on the validity of a numerical model (or its parameterisation),
69 or it could provide a physical basis for questioning the plausibility of empirically-driven interpretations or specific
70 lines/data points of evidence given that they are associated with inherent uncertainties. In order to maximise the
71 benefit to all users, any comparisons between palaeo-ice sheet model output and empirical data should ideally
72 consider the inherent uncertainties of both.

73 Given the wide availability of compilations of geochronological data (e.g. Dyke, 2004; Hughes et al., 2011;
74 Hughes et al., 2016), as well as the proliferation of ice sheet models (e.g. Greve, 1995; Rutt et al., 2009; Pollard
75 and DeConto, 2009; Winkelmann et al., 2011; Gudmundsson et al., 2012; Cornford et al., 2013; Pattyn, 2017), a
76 convenient, reproducible and consistent procedure for comparison should be of great utility to the palaeo-ice sheet

77 community. The typical volume of geochronological constraints (several thousands) for a palaeo ice sheet and the
78 number of ensemble runs (several hundreds) from an ice sheet model make a visual matching of data and model
79 output nearly impossible to accomplish, which is likely to explain the rarity of such comparisons. Here, we present
80 an Automated Timing Accordance Tool (ATAT, version 1.1). ATAT a systematic means for comparing ice-sheet
81 model output with geochronological data, which quantifies the degree of fit between the two. To separate model
82 uncertainty from data error, a single run of ATAT focuses on the error in geochronological data. This is achieved
83 by comparing geochronological data and its associated error to predictions of ice cover from single ice sheet model
84 output. However, through multiple comparisons against all members from an ensemble ice-sheet modelling
85 experiment, parameter uncertainty can be considered by assessing the degree of fit to the various input parameter
86 combinations. Therefore, ATAT could be used as a basis for examining whether model-data mismatch is a
87 consequence of inadequacies in either the model or data. The tool is in the form of a Python script and requires
88 the installation of open-source libraries. ATAT is written to handle NETCDF data as an input, a format commonly
89 used in ice sheet modelling and is also accessible from many GIS packages in which geochronological data can
90 be stored and manipulated.

91 **2 Background**

92 Geochronological evidence and ice sheet model outputs are often independently used to reconstruct the timing of
93 glaciological events. The two approaches are fundamentally different in nature and consequently produce
94 contrasting data outputs. Thus, before describing our approach to comparing the two sets of data (ATAT), we first
95 briefly consider the nature of both geochronological data and ice-sheet model output to highlight the issues and
96 potential difficulties associated with comparing the two and conceptualise a comparison procedure. More
97 extensive descriptions of the nature, uncertainties and limitations of glacial geochronological (Hughes et al., 2016;
98 Small et al., 2017) and model-based (Rougier, 2007; Tarasov et al., 2012; Briggs and Tarasov, 2013) data are
99 considered elsewhere. Given the complex nature of both, those seeking to compare geochronological data and
100 ice-sheet model output should ideally collaborate with those who understand the limitations and uncertainties
101 involved with both forms of data.

102 **2.1 Geochronological data**

103 The timing of palaeo-ice sheet activity has primarily been dated using three techniques: (i) radiocarbon dating;
104 (ii) cosmogenic nuclide exposure dating, and (iii) luminescence dating (Figure 1). The utility of each method for
105 determining the timing of palaeo-ice sheet activity has been extensively reviewed elsewhere (e.g. Fuchs and
106 Owen, 2008; Balco, 2011; Small et al., 2017) and only a brief description is provided here. Radiocarbon dating
107 uses the known rate of the radioactive decay of ^{14}C to determine the time elapsed since the death of organic
108 material (Libby et al., 1949; Arnold and Libby, 1951; Figure 1). For palaeo-glaciological purposes, the dated
109 organic material (e.g. shells, mosses, plant remains) is usually taken from basal sediments overlying and closely
110 associated with a glacial deposit in order to determine a minimum deglaciation age (e.g. Heroy and Anderson,
111 2007; Lowell et al., 2009); ice is interpreted to have retreated from this site some short time prior to this age.
112 Where organic matter is either reworked within or is located directly beneath a glacial deposit, it can be used to
113 constrain the maximum age of glacial advance (e.g. Brown et al., 2007; Ó Cofaigh and Evans, 2007); advance

114 happened sometime after this age. Cosmogenic nuclides (e.g. ^{10}Be , ^{26}Al and ^{36}Cl) are produced by the
115 interaction of secondary cosmic radiation in minerals, such as quartz, within materials exposed at the Earth's
116 surface (Figure 1). Samples are generally taken from glacially-transported boulders, morainic boulders and
117 glacially modified bedrock, all of which have ideally had signals from any previous exposure history removed by
118 glacial erosion. Cosmogenic nuclide dating is thus used to determine the duration of time a sample has been
119 exposed at the Earth's surface by determination of the concentration of cosmogenic nuclides within that sample.
120 Luminescence dating can determine the age of a deposit by measuring the charge accumulated within minerals.
121 This charge accumulates in light-sensitive traps within the crystal lattice due to ionizing radiation produced by
122 naturally occurring radioactive elements (e.g. U, Th, K). Luminescence dating determines the time elapsed since
123 the last exposure of the mineral to sunlight; this exposure acts to reset the signal (Figure 1). As subglacial deposits
124 are unlikely to have been exposed to light before burial, and therefore contain signals accumulated prior to
125 deposition, luminescence dating within palaeo-glaciology is typically applied to ice marginal sediments, or those
126 which overly glacial sediments (e.g. Duller, 2006; Smedley et al., 2016; Bateman et al., 2018). All
127 geochronological techniques record the absence of grounded ice. They therefore provide either maximum or
128 minimum ages of a glaciological event, depending upon the stratigraphic setting. Table 1 outlines a commonly
129 used system used to classify geochronological data by stratigraphic setting (Hughes et al., 2011; 2016).

130 The retreat/advance (ice-free) ages provided by the three geochronometric techniques are all affected by
131 systematic and geological uncertainties (Small et al., 2017). Systematic uncertainties originate from the tools and
132 techniques used to derive the date, such as laboratory instruments and sample preparation, and are accounted for
133 in the quoted errors that accompany a date. Geological uncertainties are caused by the geological history of a
134 sample, before, during and after a glacial event (e.g. Lowe and Walker, 2000; Lukas et al., 2007; Heyman et al.,
135 2011). Such influences may leave little or no evidence of their effect upon a sample and are thus hard to quantify.

136 The relationship between a dated sample and the glacial event it indicates is the largest potential source of
137 uncertainty in geochronological data and is primarily bounded by the ability of the investigator to find and
138 associate dateable material to the glacial event of interest. Since all geochronological techniques measure the
139 absence of ice, expert inference must be made, and are influenced by the availability of information (stratigraphic
140 or otherwise) at a study site; they may be open to change (e.g. new radiocarbon calibrations, new cosmogenic
141 isotope production rates). Furthermore, in the cases of luminescence and radiocarbon dating, there can be an
142 unknown duration since glacial occupation of an area and the deposition of dateable material. These factors mean
143 it is necessary to consider the quality of dates for ascertaining the timing of the glacial event in question (Small et
144 al., 2017).

145 Numerous geochronological studies have sought to ascertain the timing of palaeo-ice sheet activity at sites, leading
146 to compilations of geochronological data which bring together hundreds to thousands of published dates (e.g.
147 Dyke et al., 2002; Livingstone et al., 2012; Hughes et al., 2011; 2016). Despite the growing number of reported
148 dates, they are still insufficient in number and spatial spread to define, on their own, the time-space envelope of
149 the shrinking ice sheet. Techniques to interpolate geochronological information between sites are required. The
150 most commonly used technique is empirical ice sheet reconstruction (e.g. Dyke, 2004; Clark et al., 2012), whereby
151 expert assessments of the geochronological and geomorphological record are used together to create ice-sheet
152 wide isochrones of ice-sheet margin position and flow configuration. A recent advance in this method has been
153 the inclusion of confidence envelopes for each isochrone, documenting possible maximum, likely and minimum

154 extents (Hughes et al., 2016). Further techniques for spatiotemporally interpolating geochronological data include
155 Bayesian sequence modelling (e.g. Chiverrell et al., 2013; Smedley et al., 2017), in which collections of deglacial
156 ages are arranged in spatial order determined by a priori knowledge of geomorphologically-informed ice flow and
157 retreat patterns (e.g. Gowan, 2013). Such techniques provide viable methods for producing ice-sheet wide
158 chronologies, filling in information in locations where geochronological data may be sparse.

159 **2.2 Ice sheet model output**

160 Ice-sheet models solve equations for ice flow over a computational domain, for a given set of input parameters
161 and boundary conditions, to determine the likely flow geometry and extent of an ice sheet. Typically, ice-sheet
162 models run using finite difference techniques on regular grids (e.g. Rutt et al., 2009; Winkelmann et al., 2011).
163 Ice-sheet models that utilise adaptive meshes (e.g. Cornford et al., 2013) and unstructured meshes also exist (e.g.
164 Larour et al., 2012) and the results from such models can be interpolated onto spatially regular grids. The spatial
165 resolution of an ice-sheet model depends upon the computational resources available, and the spatial resolution
166 of available boundary conditions. Continental-scale models of palaeo-ice sheets have typical spatial resolution of
167 tens of kilometres (e.g. Briggs and Tarasov, 2013; DeConto and Pollard, 2016; Patton et al., 2016), though parallel,
168 high-performance computing means higher resolutions are possible (e.g. 5 km in Gollledge et al., 2013 and
169 Seguinot et al., 2016). The temporal resolution of ice sheet model output is ultimately limited by the time-steps
170 imposed by the stability properties of the numerical schemes solving the ice-flow equations. Given that these
171 stable time-steps can be sub-annual, output frequency is mostly predetermined by the user (typically decades to
172 centuries), and as such is constrained by available disk-storage. Ice-sheet models therefore produce spatially
173 connected predictions of ice-sheet behaviour such as advance and deglaciation (e.g. Table 1) across gridded
174 domains at various temporal and spatial resolutions.

175 The stress fields imposed upon ice can be fully described by solving the Stokes equations. Indeed, 'full Stokes'
176 models which do so have been tested (Pattyn et al., 2008) and used to simulate ice sheets (e.g. Seddik et al., 2012).
177 However, fully solving the Stokes equations over the spatio-temporal scales relevant to palaeo-ice sheet
178 researchers remains beyond the limit of currently available computational power. This problem is exacerbated by
179 the need to run multi-parameter valued ensemble simulations to account for model uncertainty over multi-
180 millennial and continental-scale domains. This means that palaeo-ice sheet modelling experiments rely upon
181 approximations of the Stokes equations (see Kirchner et al., 2011 for a discussion), such as the shallow ice
182 approximation (SIA) and shallow shelf approximation (SSA). The choice of ice-flow approximation used within
183 a model has implications for the capability of models to realistically capture aspects of ice sheet flow (Hindmarsh,
184 2009; Kirchner et al., 2011; 2016), and in turn influences the nature of the model output produced. For instance,
185 the SIA is not applicable for ice shelves, therefore SIA-based models do not produce modelled ice shelves (e.g.
186 Glimmer; Rutt et al., 2009). Therefore, the timing of deglaciation in an SIA model can be determined as the point
187 at which ice thickness in a cell becomes zero or thinner than the flotation thickness, whereas in a SSA or higher-
188 order model the location and movement of the grounding line must be determined.

189 Though ice sheet models produce output which is consistent with model physics, like all numerical models of
190 physical systems (e.g. Rougier, 2007) there are many sources of uncertainty involved with ice sheet modelling.
191 Three broad sources of model-based uncertainty can be distinguished: (i) down-scaling; (ii) parametric
192 uncertainty; (iii) structural uncertainty. These are defined and discussed below.

193 Down-scaling uncertainties arise due to an ice-sheet models computation over space which has a coarser resolution
194 than reality. This means that a characteristic which can be measured to a high level of accuracy and precision for
195 a real ice-sheet (e.g. the position of a calving front), has a larger uncertainty in an ice-sheet model. This is
196 especially pertinent for data-model comparisons, as most observations of ice-sheet activity have a sub-model
197 resolution.

198 Parametric uncertainty has two main sources: (i) parameterisations, and (ii) boundary conditions. Where a process
199 is too complex (e.g. calving) or occurs at too small a scale (e.g. regelation) to be captured by an ice sheet model,
200 it is often simplified and parameterised. Associated with each parameterisation are a set of parameters, the values
201 of which are either unknown, or thought to vary within some plausible bounds, and which can either be constant
202 or spatially and temporally variable across a domain. An example of a process which is often parameterised is
203 basal sliding. This parameterisation is often done through the implementation of a sliding law (e.g. Fowler, 1986;
204 Bueler and Brown, 2009; Schoof, 2010), which relates the basal shear stress to the basal velocity (Fowler, 1986).
205 Parameters used to determine this relationship are often assigned or incorporated within a parameter, or prescribed
206 by another model parameterisation (e.g. a subglacial hydrology model). Adding to the uncertainty in the absence
207 of a single preferable sliding law, ice-sheet models often allow the user to choose between different sliding law
208 implementations.

209 Boundary conditions, the values prescribed at the edge of the modelled domain, also introduce uncertainty into
210 ice-sheet models. For contemporary ice sheets, there is a large uncertainty in the basal topography (e.g. Fretwell
211 et al., 2013). This is less of a problem for the more accessible beds of palaeo-ice sheets. However, accurately
212 accounting for the evolution of this bed topography over the course of a glaciation requires a model of isostatic
213 adjustment (Lingle and Clark, 1985; Gomez et al., 2013).

214 A very large source of uncertainty for modelling palaeo-ice sheets is the climate used to drive them (Stokes et al.,
215 2015), as indeed is the case for forecasts of contemporary ice sheets (e.g. Edwards et al., 2014). Owing to the
216 computational resources required and technical challenges, few palaeo-ice sheet models are coupled with climate
217 models. This uncertainty over past climate is reflected in the large range of outputs produced by global circulation
218 models which have tried to simulate the last glacial cycle (e.g. Braconnot et al., 2012). Palaeo-ice sheet modellers
219 have used a range of methods to force their models, including simple parameterisations (Boulton and Hagdorn,
220 2006), applying offsets derived from ice core records to contemporary climate (e.g. Huybrechts, 1990; Hubbard
221 et al., 2009) and scaling between present-day conditions and uncoupled global-circulation-model simulations at
222 maximum glacial conditions (e.g. Greve et al., 1999; Gregoire et al., 2012; Gasson et al., 2016). Each approach is
223 associated with an inherent uncertainty. When this uncertainty is accounted for in an ensemble experiment, the
224 range of possible climates produces numerous ice sheet outputs.

225 Structural uncertainty is related to parametric uncertainty, but has a broader remit, and is defined as uncertainty
226 which occurs due to differences in model coding and design (Collins, 2007; Tebaldi and Knutti, 2007). This
227 encompasses differences in which processes are included in different models, and also the manner in which they
228 are implemented. Structural uncertainty is difficult to quantify, but can be explored by multi-model comparison
229 (Murphy et al., 2004; Collins et al., 2011). Such comparisons are not currently routine in palaeo-ice sheet
230 modelling. Differences in model coding (i.e. structural uncertainty), arise due to a lack of understanding regarding
231 the physical system in question. This points to a broader uncertainty with a similar remit, that no models can

232 ~~include processes that are as yet unknown to science. Reducing this source of uncertainty is an ongoing challenge~~
233 ~~for glaciology.~~

234 ~~Structural uncertainty is related to parametric uncertainty, but has a broader remit, and is defined here as all~~
235 ~~uncertainty that arises within a model due to a lack of physical understanding of the system in question. In this~~
236 ~~broad sense, structural uncertainty encompasses all processes which are not incorporated in a model. This may~~
237 ~~include some processes which are well understood, but not included in a model due to the lack of a numerical~~
238 ~~formulation, for computational efficiency, or because they are deemed unimportant for the question being studied.~~
239 ~~In a broader sense, structural uncertainty also includes processes that are as yet unknown to science and therefore~~
240 ~~are not implemented in a model. Reducing structural uncertainty, by including additional pertinent processes in~~
241 ~~models, is an ongoing challenge for ice-sheet modelling.~~

242 There is another ~~structural~~ uncertainty - which hinders ice-sheet models from being able to accurately predict the
243 evolution of ice-sheets, which is the presence of instabilities – we use this term in the technical sense of a small
244 perturbation that leads to the whole ice-sheet system amplifying this small perturbation to the extent it can leave
245 a mark in the geological record. A classic example of this in ice-sheet dynamics is the marine ice-sheet instability
246 (MISI), first discussed in the 1970s (Hughes, 1973; Weertman, 1974, Mercer, 1978) and more recently put on a
247 sounder mathematical footing (Schoof 2007, 2012).

248 The MISI actually refers to an instability in grounding-line (GL) position on a reverse slope, where the water
249 depth is shallowing in the direction of ice flow. Since ice flux increases with ice thickness, a straightforward
250 argument leads to the conclusion that if the GL advances into shallower water, the efflux will decrease, the ice
251 sheet will gain mass and the advance continue. If, on the other hand, the GL retreats, the flux will increase, the
252 ice-sheet will lose mass and the retreat continue. In principle, given the right parameterisations and basal
253 topography, ice-sheet models should be able to predict the ‘trajectory’ of GL migration arising as a consequence
254 of the MISI. However, the MISI is one of the class of instabilities that lead to poor predictability; certain small
255 variations of parameters and specifications will lead to large-scale changes in the ‘trajectory’, in this case the
256 retreat history. A well-known analogy is the ‘butterfly effect’, which originated in atmospheric modelling work
257 (Lorenz, 1963); the butterfly effect is concerned with the consequences of the statement “small causes can have
258 larger effects”. Recent work has also shown that additional physical processes, such as ice-shelf buttressing
259 (Gudmundsson, 2012) and the effect that the gravitational pull of ice-sheets has on sea level (Gomez et al., 2012)
260 have additional effects on grounding line stability. Given that most of the palaeo-ice sheets during the last glacial
261 cycle had extensive marine margins and overdeepened basins, with isostatic adjustment creating further zones of
262 reverse slope, capturing grounding line processes is important for simulating these ice-sheets.

263 **2.3 Considerations when comparing geochronological data and ice-sheet model output**

264 Sections 2.1 and 2.2 make it clear that several factors must be considered in order to satisfactorily compare
265 geochronological data and ice-sheet model output (Table 2). Most critically, the two datasets involved in any
266 comparison have varying spatial properties. Raw geochronological data is unevenly distributed and located at
267 specific points, with horizontal position accurate to a metre or so; such data may be used to plot ice-margin
268 fluctuations of the order of tens of kilometres (Figure 2C). Ice-sheet models typically produce results on evenly-
269 spaced points (at ~5 km to 20 km resolution) that are distributed over and beyond the maximum area of the palaeo-
270 ice sheet (Table 2; Figure 2B). Consequently, in comparing the two, a choice must be made; either

271 geochronological data should be gridded (coarsened) to the resolution of the ice-sheet model, or the ice-sheet
272 model results must be interpolated to a higher resolution. Both options have drawbacks, as the former removes
273 spatial accuracy from geochronological data while the latter relies upon interpolation beyond model resolution
274 and, more seriously, model physics. A second problem lies in the spatial organisation of the data (Table 2). Ice-
275 sheet models produce a regular grid of data (Figure 2B), meaning that no location is more significant than any
276 other when comparing the modelled deglacial chronology with that inferred from geological data. Conversely,
277 owing to the uneven distribution of raw geochronological data, some regions of a palaeo-ice sheet may be better
278 constrained than others (Figure 2C). As noted by Briggs and Tarasov (2013), any comparison that does not treat
279 the uneven spatial distribution of geochronological data may favour sites where numerous dates exist over more
280 isolated locations. One approach to overcoming these disparities is to use an interpolation scheme (e.g. empirical
281 reconstruction, Bayesian sequence) on the raw geochronological data. This produces a geochronological
282 framework by combining evidence on pattern and timing to yield a distribution that is spatially more uniform and
283 a spatial resolution similar to that of palaeo-ice sheet model output (Figure 2D).

284 The temporal intervals between and precision of geochronological data and ice sheet model output also vary
285 (Table 2). The time intervals between geochronometric data are determined by the number of available
286 observations, and precision determined by sources of uncertainty. Conversely, ice sheet models produce output at
287 regular intervals and are temporally exact, which is to be contrasted with 'correct'. Since the output interval of an
288 ice-sheet model is generally determined by the user (see Section 2.2) it is pertinent to consider an appropriate
289 time-interval of ice-sheet model output for comparison with geochronological data. For example, radiocarbon
290 dates have precision typically in the order of hundreds of years but do not directly constrain ice extent, whilst
291 empirically reconstructed isochrones are typically produced for thousand-year time-slices (e.g. Hughes et al.,
292 2016). In reality, ice-sheets may respond to events at faster time-scales than this, but in the absence of internal
293 instabilities (e.g. MISI) palaeo-ice sheet models are ultimately limited by the temporal resolution of the available
294 climate forcing data. Thus, to gain insight into controls on palaeo-ice sheet behaviour, it may be necessary to
295 create model output with a greater (centurial) temporal resolution than the uncertainty associated with
296 geochronology.

297 Both geochronological data and ice-sheet model output have sources of uncertainty which must also be considered
298 when comparing the two. For geochronological data, uncertainty is typically expressed as a standard deviation
299 from the reported age, and are therefore easy to consider when comparing to an ice sheet model. For ice-sheet
300 models, individual model runs do not currently express uncertainty, and it is only when multiple, ensemble, runs
301 which systematically vary parameters and boundary conditions are conducted that uncertainty in all output
302 variables can be expressed. Therefore, any comparison between geochronological data and model simulations
303 must either compare to all members of an ensemble experiment in turn, or against a amalgamated output from an
304 ensemble which considers model uncertainty. Having said this, statistical techniques exist to derive probability
305 distribution functions for individual quantities (e.g. Ritz et al., 2015). Such ensemble runs typical comprise
306 hundreds to thousands of individual runs (Tarasov and Peltier, 2004; Robinson et al., 2011). Given the volume of
307 data this produces, one appealing application of a quantitative comparison between geochronological data and ice
308 sheet model output would be to act as a filter for scoring ice-sheet model runs and reducing predictive uncertainty
309 by only using the parameter combinations that were successful. However, if all possible parameters have been
310 modelled, (i.e. the full 'phase-space' of the model has been explored (cf. Briggs and Tarasov, 2013)), and very

311 few (or no) model runs conform to a certain set of geochronological data or an empirical reconstruction, this may
312 provide a basis to question aspects of the evidence (e.g. re-examining the stratigraphic context of a dated sample
313 site or questioning the basis of the reconstructed isochrone). Of course, a third possibility that both data and model
314 are incorrect cannot be excluded.

315 We therefore suggest that any comparison between ice-sheet model experiments and geochronological data should
316 consider:

- 317 i) That both ice-sheet models and geochronological data have inherent uncertainties;
- 318 ii) That geochronological data typically provide a constraint on just the absence of ice; such that ice must have
319 withdrawn from a site sometime (50 years? 500 years? 5000 years?) prior to the date (which can be any point
320 within the full range of the stated uncertainty). It is thus a limit in time and not a direct measure of glacial activity.
321 Figure 3 illustrates this for advance and retreat constraints. It is most often the case that dated material is taken
322 close to the stratigraphic boundary or landform representing ice presence, in which case a date might be considered
323 as a 'tight constraint' (e.g. the ice withdrew and very soon afterwards (50 years) marine fauna colonised the area
324 and deposited the shells used in dating). Sometimes however there may have been a large (centuries to millennia)
325 interval of time between the withdrawal and the age of the shell chosen as a sample, in which case the date will
326 provide a 'loose' limiting constraint; it might be much younger than ice retreat (Figure 3).
- 327 iii) There is inherent value to the expert interpretation of stratigraphic and geomorphological information, meaning
328 an ice-free age reported for a site is likely as close as possible (tight constraint) to a glacial event. However, this
329 interpretation could be subject to change;
- 330 iv) Geochronological data exist as spatially distributed dated sites (e.g. Figure 2C) which can be built into a
331 spatially coherent reconstruction (e.g. Figure 2D);
- 332 v) A great input uncertainty in a palaeo-ice sheet model is the climate, which can lead to changes in the spatial
333 extent and timing of ice sheet activity.
- 334 vi) A factor which requires further investigation is the relationship between the operation of a physical instability
335 (e.g. the MISI) and the practical ability of models to predict retreat or advance rates; the presence of an instability
336 can result in extreme sensitivity to parameter ignorance or over-simplified model physics.
- 337 vii) Other uncertainties can also lead to variations in ice-sheet model results; these can be accounted for in an
338 ensemble of hundreds to thousands of simulations.

339 Given the above, it is unlikely that a single procedure could capture model-data conformity. ATAT therefore
340 implements several ways of measuring data-model discrepancies and produces output maps (described in the
341 following two sections) to help a user assess which model runs best agree with the available geochronological
342 data. One approach is to transform the geochronological data points (x,y,t) to a gridded field (raster) that define
343 age constraints of ice advance and another grid for retreat. Both of these data types also require an associated grid
344 that reports the uncertainty range as error (Figure 4). These age grids may then be quantitatively compared to
345 equivalent grids (age of advance grid and age of retreat grid) derived from the ice sheet model outputs.
346 Alternatively, one might prefer to compare model runs against the geochronological data (points) combined with
347 expert-sourced interpretive geomorphological and geological data, in which age constraints from dated sites have
348 been spatially extrapolated using moraines and the wider retreat pattern. In this case ATAT allows the model
349 outputs to be compared to the 'lines on maps' type of reconstruction subsequent to conversion from age isolines
350 to a grid of ages (Figure 4).

351 **3. Description of tool**

352 ATAT is written in Python, and utilises several freely available modules. Access to these modules may require a
353 Python package manager, such as 'pip' or 'anaconda'. ATAT can therefore be run from the command line on any
354 operating system, or by using a Python interface such as IDLE.

355 **3.1 Required data and processing**

356 ATAT requires two datasets as an input: (i) an ice-sheet model output; and (ii) gridded geochronological data.
357 Table 3 provides the required variables and standard names for each dataset. In order to determine the advance
358 age or deglacial age predicted by the ice sheet model, ATAT requires either an ice thickness (where the model
359 does not produce ice shelves) or a grounded ice-mask variable (where ice shelves are modelled). In the latter case,
360 the user is asked to define the value which represents grounded ice.

361 Empirical advance and deglacial geochronological data (Table 1) require separate input files (NETCDF format),
362 as model-data comparison for these two scenarios are run separately in ATAT. Table 1 and further references
363 (Hughes et al., 2011; 2016; Small et al., 2017), provide information regarding identification of the stratigraphic
364 setting of these two glaciological events as considered by ATAT. ATAT requires that geochronological data
365 (advance or deglacial) are interpolated onto the same grid projection and resolution as the ice-sheet model before
366 use. Though an imperfect solution to the problem of comparing grids of different resolution, (Section 2.3; Table
367 2), this was preferred to the alternative solution of regridding an ice sheet model onto a higher resolution grid, as
368 this may introduce the false impression of high resolution modelling sensitive to boundary conditions (e.g.
369 topography) beyond the actual model resolution.

370 Preparation of the geochronological data to be the same format and grid resolution as the ice sheet model output
371 requires use of a GIS software package such as ESRI ArcMap or QGIS. Users must define deglacial/advance ages
372 based either upon the availability of geochronological data in a cell, or based upon an empirical reconstruction
373 (Figure 4). These ages must be calibrated to a calendar which is the same as that output by the ice-sheet model (in
374 our case the 365-day calendar in units of seconds since 1-1-1). Where there are no data (i.e. outside the ice-sheet
375 limit), the grid value must be kept at 0. When multiple dates are contained within a cell, expert judgement is
376 required to ascertain which date is most representative of the deglaciation of a region. This assessment should be
377 based upon the quality of sample taken; criteria for establishing this quality are considered in Small et al. (2017).
378 In the case where a profile of dates has been collected (for example up a vertical section at the side of a valley, or
379 from multiple depths of a marine core) the date which most closely defines the timing of final deglaciation of an
380 area should be chosen, as this is the focus of ATAT. The assembly of this geochronological database input into
381 ATAT should consider the reliability of ages, removing outliers and unreliable ages (see Small et al. (2017) for a
382 discussion of this issue). In particular, loose constraints, such as cosmogenic dates which display inheritance or
383 radiocarbon dates effected by a depositional hiatus, should be removed as this have the potential to bias results.
384 In a comparable manner, the attribution of error to each cell is also reliant upon expert interpretation. The
385 magnitude of error may vary between the source of geochronological data (radiocarbon, cosmogenic nuclide or
386 luminescence) and user choice for experimental design (e.g. 1, 2 or 3 sigma). A single error value must be given
387 for each dated cell, corresponding to the maximum threshold beyond which the user deems it is unacceptable for
388 a model prediction to occur (Figure 3). Given that creating this input data may involve many expert decisions (e.g.
389 which date has the relevant stratigraphic setting, which date(s) are most reliable?), this part of the process is not

390 yet automated within ATAT. This data preparation stage is therefore the most time-consuming and user-intensive
391 part of the process. However, users only need to define the data-based advance/deglacial grid once to compare to
392 multiple model outputs. Future work should consider alternatives means of choosing dates and identifying outliers,
393 such as Bayesian age modelling (e.g. Chivverell et al., 2013). The input data NetCDF file should also contain the
394 variables latitude, longitude, base topography (the topography that the ice-sheet modelling is conducted on and
395 the elevation of the geochronological sample (Table 3).

396 ATAT is called from a suitable python command-line environment, using several system arguments to define
397 input variables (Table 1; Figure 5). Users must define whether they are testing a deglacial or advance scenario.
398 ATAT only considers the last time that ice advances over an area. Therefore, caution must be undertaken when
399 defining advance data in regions where multiple readvances occur, and users should consider limiting the time
400 interval of the ice sheet model tested when examining specific events (e.g. a well-dated readvance or ice sheet
401 build-up). The location of the file containing the geochronological data grid (e.g. Figure 5) is then required. From
402 this file, the age and error grids are converted to arrays. For the age data, null values are masked out using the
403 nummys masked array function. A second array that accounts for error is then created, the properties of which
404 depends upon whether a deglacial or advance scenario is being tested. For a deglacial scenario, a model prediction
405 will be unacceptable if the cell is ice-covered after the range of the date error is accounted for, but the cell may
406 become deglacialated any time before this. Therefore, the associated error value is added onto the cell date, to create
407 a maximum age at which a cell must be deglacialated by to conform to the ice sheet model (Figure 3). The opposite
408 is true for advance ages; ice can cover a cell any time after the date and associated error, but cannot cover the cell
409 before the date of the advance. In order to allow for advances which occur after the date and its error, associated
410 error is therefore subtracted from the date cell (Figure 3). To account for the uneven spatial distribution of dates,
411 a weighting for each date is then calculated based upon their spatial proximity. This weighting is used later when
412 comparing the data to the model output. To calculate this weighting (w_i), ATAT defines a local spatial density of
413 dated values based upon a kernel search of 10 neighbouring cells.

414 The user must define the path to the ice sheet model output, from which the modelled deglacial age will be
415 calculated and eventually compared to the data (Figure 4). The user must also define whether to base deglacial
416 timing on an ice thickness or grounded extent mask variable (Table 2). If the user selects thickness, the margin is
417 defined by an increase from 0 ice thickness. For the mask, the user is also asked to supply the number which refers
418 to grounded ice extent. The timing of advance is then determined by the change of a cell to this number (Figure
419 5). The margin position recreated by the ice-sheet model has a spatial uncertainty due to downscaling issues and
420 fluctuations which may occur between recorded outputs. To account for this, ATAT calculates a second set of
421 modelled deglacial ages, whereby the deglacialated region at each modelled time output is expanded to all cells
422 which neighbour the originally identified deglacialated or advanced over cells. Furthermore, the spatial resolution
423 of ice-sheet models typically means that the emergence of ice-free topography at the edge or within an ice-sheet
424 (e.g. in situations such as steep-sided valleys or nuntaks) are poorly represented. To account for this, ATAT firstly
425 calculates the modelled ice-sheet surface at each time output by adding ice thickness to the input base topography.
426 Where the modelled surface elevation is below that of the sample elevation, these cells are identified as being
427 deglacialated (Figure 5). The downscaling of topography onto ice-sheet model grids also introduces a vertical
428 uncertainty. This is accounted for in ATAT through calculating the difference between sample elevation and the

429 reference elevation. A second metric which identifies cells as having been deglaciated if they are also within this
430 vertical uncertainty is also calculated (Figure 5).

431 3.2 Model-data comparison

432 Once the required variables have been retrieved from the NETCDF data and manipulated, ATAT compares the
433 geochronological age and modelled age at each location (Figure 4). Firstly, the grid cells which have data are
434 categorised as to whether there is model-data agreement, based on the criteria shown in Figure 3. Since all dating
435 techniques only record the absence of ice, geochronological data provides only a one-way constraint on palaeo-
436 ice sheet activity. For deglacial ages, deglaciation could occur any time before the geochronological data provided
437 and within the error of the date (i.e. deglacial ages are minimum constraints), but deglaciation must not occur after
438 the error of the date is considered (Figure 3). For advance ages, advance must have happened after the date or
439 within error beforehand (i.e. advance ages are maximum constraints), but palaeo-ice sheet advance cannot occur
440 in the time period before that dated error (Figure 3). Once ATAT has determined whether each cell conforms to
441 these criteria, a map is produced identifying at which locations the ice sheet model agrees with the
442 geochronological data.

443 Though the criteria described above and illustrated in Figure 3 allow for the identification of dates which conform
444 to the predictions of an ice sheet model, they provide little insight into how close the timing of the model prediction
445 is to the geochronological data. If these were the only criteria on which a model-data comparison was made, it
446 could prove problematic. In an extreme case, one could envisage that all retreat dates are adhered to by a model
447 run that deglaciates from a maximum extent implausibly rapidly (say 50 years!), and, given that we only have
448 one-way (minimum) constraints on deglaciation (Figure 3), this model run would conform to all modelled dates.
449 Whilst the nature of geochronological data (being only able to determine the absence of ice) does not preclude
450 such a scenario, this assumes that there is no inherent value to the expert judgement and stratigraphic interpretation
451 of each date as being close to palaeo-ice sheet timing (cf. Small et al. 2017). Therefore, ATAT also determines
452 the temporal proximity of the geochronological data and the model prediction. Firstly, a map of the difference
453 between modelled and empirical ages is created (Figure 5). This enables the identification of dates which are a
454 large distance away from the model prediction. Secondly, the route-mean square error (RMSE) is calculated using
455 the Eq. (2):

$$456 \quad RMSE = \sqrt{\frac{1}{n} \sum_{i=1}^n (g_i - m_i)^2},$$

457 (1)

458 where n is the number of cells which contain empirical geochronological information, g_i is the associated
459 geochronological date, and m_i is the model predicted age. The RMSE works well when the geochronological
460 data is evenly spatially distributed, either from a reconstruction (i.e. isochrones) or a wealth of dates. ATAT also
461 calculates a weighted RMSE (wRMSE), for situations where this is not the case (i.e. there is a paucity of dates
462 that are not distributed evenly across the domain) using Eq. (3):

$$463 \quad wRMSE = \sqrt{\frac{1}{n} \sum_{i=1}^n ((g_i - m_i)/w_i)^2},$$

464 (2)

465 where w_i is the spatial weighting factor. Results of the RMSE and wRMSE calculations are separated by the
466 degree to which included dates agree with model output. This creates an array of metrics with varying levels of
467 consideration of model and data uncertainty (Figure 5). Both the RMSE and wRMSE are calculated for all dates,
468 to create a metric that doesn't account for dating error but may give an indication of how close a model-run gets
469 to dated cells. Dated locations are also categorised according to whether model-data agreement occurs within
470 dating error, and whether the addition of horizontal (ice margin) and vertical (ice surface) downscaling uncertainty
471 means that model-data agreement occurs. The RMSE and wRMSE are calculated for these categories to create a
472 metric which accounts for data and model uncertainty (Figure 5), and also for those dates which where model-
473 data agreement within dating error occurs to create a metric which does account for model-error (Figure 5). ATAT
474 then produces a .csv file containing all calculated statistics per ice-sheet model output file. We suggest that the
475 most rigorous metric, the wRMSE of dates which conform within geochronological data and model downscaling
476 uncertainty (Figure 5), should most frequently used. However, other metrics, such as the RMSE of all dates, may
477 give an indication of performance earlier in the modelling process. For example, initial results may reveal that no
478 or very few dates conform to a set of model simulations within model and data uncertainty, but the RMSE of all
479 dates may give an indication of models and associated parameters to be explored further. Given the complexity
480 of data-model comparison, different statistics may have different uses. For instance, the percentage of covered
481 dates may prove useful to identify the worst performing model runs (i.e. the bottom 50%), whilst the wRMSE of
482 dates within error may be more convenient for choosing between model runs. However, given the uncertainty in
483 ice-sheet modelling it is likely that in an ensemble there will be no single model run which has significantly better
484 metrics than others, so ATAT may best be used to choose members which pass a user-defined threshold of
485 combined metrics.

486 Pragmatically, we envisage that ATAT could be used in the following ways, though others may exist. In sensitivity
487 experiments (e.g. Huybrechts, 1990; Hubbard et al., 2009; Patton et al., 2016), ATAT could be used to quantify
488 how the alteration of a parameter influences the fit of a model to geochronological data. In ensemble experiments,
489 ATAT could be used to rank the performance of individual ensemble member simulations with respect to
490 geochronological constraints, either as a means of ruling out simulations with the poorest performance (e.g.
491 Gregoire et al., 2012) or calibrating input parameters for further experiments (e.g. Tarasov et al., 2012). Where
492 the results of an ensemble experiment have been amalgamated (i.e. where each cell has a distribution of ice-free
493 ages), ATAT could be compared to measures of average modelled deglaciation/advance age and against standard
494 deviations of these. Such comparisons could reveal areas of persistent model-data mismatch. If this is the case,
495 this may form the basis of identifying regions of significant model uncertainty (does this site not match due to
496 poor implementation of processes in the model?) or form the basis for re-examination of the geological evidence
497 (are there reasons why this site is consistently an outlier?). Furthermore, ATAT could be used to explore how
498 incorporating additional processes into a model alter the fit to data. Here, we envisage two sets of model
499 experiments, one which includes a new implementation of a process in a model and another which does not
500 implement this process, whilst holding all other things equal between the two experiments. ATAT could then be
501 used to distinguish whether a better fit to geochronological data can be made when the new process is accounted
502 for.

503 **4. Application of tool**

504 **4.1 Ice Sheet Model**

505 To trial ATAT we used geochronological data and ice sheet modelling experiments from the former British-Irish
506 Ice Sheet (BIIS). A vast quantity of previous research has produced a high density of dates (Hughes et al., 2011)
507 which are being substantially augmented by the BRITICE-CHRONO project ([http://www.britice-
509 chrono.group.shef.ac.uk/](http://www.britice-
508 chrono.group.shef.ac.uk/)). Along with an abundance of well documented landforms (Clark et al., 2017), this
510 makes the BIIS a data-rich study area for empirical reconstructions and ice sheet modelling. Ongoing modelling
511 work aims to capture the behaviour of the BIIS inferred from the geomorphological and geochronological record
512 (see Clark et al., 2012 for a recent reconstruction). We do not expect our model to capture these specific details.
513 Instead, the purpose of modelling in this paper is merely to illustrate the use of ATAT. We therefore restrict
514 ourselves to simplified modelling experiments and show only three model runs (Experiments A, B and C), whereas
515 a full ensemble experiment would contain hundreds or thousands of simulations.

516 Ice sheet modelling experiments were conducted using the Parallel Ice Sheet Model (PISM; Winkelmann et al.,
517 2011). This is a hybrid SIA-SSA model, with an implementation of grounding line physics. It is therefore suited
518 to modelling both the marine-based portions of the BIIS and the terrestrial realm. The model simulates the history
519 of the BIIS from 40 ka to present. The model is run at 5 km resolution, with basal topography derived from the
520 General Bathymetric chart of the Oceans (www.gebco.net). This is updated to account for isostatic adjustment
521 using a viscoelastic Earth model (Bueler et al., 2007) and a scalar eustatic sea level offset based on the SPECMAP
522 data (Imbrie et al., 1984). All three model runs, labelled A-C, had the same input parameters and boundary
523 conditions, apart from climate forcing. We take a similar approach to Seguinot et al. (2016) in computing a climate
524 forcing. Modern values of temperature and precipitation are perturbed by a proxy temperature record, in this case
525 the GRIP ice core record (Johnsen et al., 1995). These are input into a positive degree day model to calculate mass
526 balance (Calov and Greve, 2005). Input precipitation values are the same between experiments. To introduce
527 variation between the experiments, temperature varies such that Experiment A is the equivalent of modern day
528 values, Experiment B has values uniformly reduced by 1°C and Experiment C has values uniformly reduced by
529 2°C. All other parameters and forcings are equal between experiments. This simple approach to climate forcing
530 here used for demonstration purposes only, and does not capture the changes to atmospheric and oceanic
531 circulation patterns that occur during a glacial cycle.

532 The maximum extent of ice for each experiment is shown in Figure 6 and the timing of advance and retreat is
533 shown in Figure 7. Potentially unrealistic ice sheets occur in the North Sea, perhaps due to the choice of domain
534 not including the influence of the Fennoscandian ice sheet in this area. As noted above, we do not expect these
535 model runs to fully replicate the reconstructed characteristics of the BIIS (e.g. Clark et al., 2012). However, it is
536 worth noting general, visually-derived, observations regarding the outputs shown in Figure 6. For larger
537 temperature offsets, the ice sheet gets bigger, the timing of maximum extent gets progressively later and the
538 modelled ice sheet gets thicker (Figure 6). In all experiments, there is generally a gradual advance toward the
539 maximum extent followed by retreat (Figure 7). This pattern is interrupted by a later readvance that corresponds
540 to the timing of the Younger Dryas in the GRIP record; this causes ice to regrow over high elevation areas such
541 as Scotland and central Wales. The extent of this readvance increases with decreased temperature offsets between
542 experiments (Figure 7). Smaller readvances, occurring around 16.5 ka also occur (Figure 7).

542 4.2 Geochronological data

543 Ice-sheet advance dates were taken from the compilation of Hughes et al. (2016) and gridded to the ice sheet
544 model domain (Figure 4). In total, 61 cells were represented with advance dates (Figure 8A). Considering now
545 ice-sheet retreat (Figure 8B), dates deemed reliable or probably reliable by Small et al. (2017) were used (i.e.
546 those given a ‘traffic light rating’ of green or amber). For the dated advance and retreat locations, the
547 geochronological data in each cell was assigned an error corresponding to that which was reported in the literature.
548 We also compared our results to the ‘likely’ empirical reconstruction of Hughes et al. (2016), based on that of
549 Clark et al. (2012) (Figure 8C), using the minimum and maximum bounding envelopes to assign an error to each
550 cell of the ice sheet grid (Figure 8D). The largest errors occur in the North Sea region, where there is a lack of
551 empirical data (e.g. Figures 8A and B).

552 4.3 Results

553 Table 4 shows selected statistics derived by ATAT when comparing the three ice-sheet modelling experiments
554 (Figures 6 and 7) against the three categories of data (Advance, Retreat, Isochrones; Figure 8). wRMSE was not
555 calculated for the DATED isochrone reconstruction, as grid points are distributed evenly and therefore have equal
556 spatial weighting (Table 4). Experiment C produces modelled ice-sheets with the greatest areal extent, and
557 therefore performs best at correctly covering the dated areas (Table 4). However, none of the three experiments
558 perform particularly well when compared with the data or the empirical reconstruction regarding timing and
559 results in high (>2000 year) RMSEs (Table 4). The application of ATAT and the results from these simplified
560 experiments allow us to suggest directions for analysing future experiments.

561 All three experiments produced large RMSEs, in the order of thousands of years, when compared to all three
562 categories of data (Table 4). For advance ages, the three simulations conform to a large number of dated locations
563 (e.g. 72% of ages in Experiments B and C; Table 4). However, the RMSEs of advance ages are high (Table 4).
564 This shows that, while the models perform well at matching the constraint of covering an area in ice after an
565 advance age (Figure 3), the models often glaciates a region much later than required. Advance dates are particularly
566 difficult to obtain from the stratigraphic record, and often there may be a long hiatus between the initial deposition
567 of datable material and the subsequent advance of a glacier. Future experiments with large ensembles should
568 therefore consider the number of advance dates conformed to (rather than the RMSE) as a more robust guide for
569 model performance during ice advance.

570 For the retreat comparisons, the three modelling experiments conform to a larger percentage of sites, seemingly
571 outperforming the empirically-derived DATED reconstruction (Table 4). However, where model-data agreement
572 occurs, the RMSE produced are much higher when the model is compared to the DATED reconstruction. This is
573 due to the reconstruction containing large uncertainties in regions which lack geochronological control (for
574 example in the North Sea, Figure 8). These uncertainties, a product of spatial interpolation across regions with
575 sparse information, are much greater than those associated with individual dates. Figure 9A shows examples of
576 output maps from ATAT which display the spatial pattern of agreement and the magnitude of the difference
577 between Experiment C and the DATED reconstruction. This shows that due to the uncertainty associated with
578 North Sea glaciation, even where the model produces an unrealistic artefact, there is data-model agreement.
579 Furthermore, ATAT produces a map which displays the number of years between data-based and modelled retreat
580 and/or advance (e.g. Figure 9B). Figure 9B, which compares Experiment C to the DATED isochrones, shows that

581 the timing of model-data disagreement is spatially variable. If more modelling simulations were conducted, such
582 maps may reveal regions of reconstruction or particular dates which are difficult to simulate in the model. In such
583 cases, data or model re-evaluation may be required and herein lies the potential utility of this ATAT tool in making
584 sense of ensemble model runs. However, such model-data comparison awaits a full-ensemble simulation which
585 accounts for model uncertainty (e.g. Hubbard et al., 2009).

586 **5. Summary and concluding remarks**

587 Here we present ATAT, an automated timing-accordance tool for comparing ice-sheet model output with
588 geochronological data and empirical ice sheet reconstructions. We demonstrate the utility of ATAT through three
589 simplified simulations of the former British-Irish Ice Sheet. Note that a larger ensemble model of hundreds to
590 thousands of runs is required for model evaluation (e.g. Hubbard et al., 2009). ATAT enables users to quantify
591 the difference between the simulated timing of ice sheet advance and retreat and those from a chosen dataset, and
592 allows production of cumulative ice coverage agreement maps that should help distinguish between less and more
593 promising runs. We envisage that this tool will be especially useful for ice-sheet modellers through justifying
594 model choice from an ensemble, quantifying error and tuning ice-sheet model experiments to fit geochronological
595 data. Ideally, this tool should be used in combination with other evaluation methods, such as fit to relative sea-
596 level records. In the case where locations or regions of data cannot be fit by a model, and all model uncertainty
597 has been accounted for in an ensemble simulation, the comparisons made in ATAT may also highlight that data
598 re-evaluation is necessary. ATAT is supplied as supplementary material to this article.

599 **6. Code Availability**

600 ATAT 1.1 source code is freely distributed under a GNU GPL licence as supplementary material to this paper. It
601 can also be downloaded with example input grids from <https://figshare.com/s/6c8f885e9d10558ed359>. An example
602 geochronological data grid and ice-sheet model grid can also be downloaded from this link. The ice sheet
603 modelling experiments shown here were conducted using the Parallel Ice Sheet Model (<http://pism-docs.org/>).
604 Development of PISM is supported by NASA grant NNX17AG65G and NSF grants PLR-1603799 and PLR-
605 1644277. The geochronological data used is freely available from
606 <https://www.sciencedirect.com/science/article/pii/S0012825216304408#s0105> and
607 <https://doi.pangaea.de/10.1594/PANGAEA.848117>.

608 **6.1. General Instructions**

609 ATAT is written in python, and distributed as both .py script, for use in Python 2, and a .py3 script, for use with
610 Python 3. The tool requires installation of Python and the following freely available Python packages:

- 611 • netCDF4 (<https://pypi.python.org/pypi/netCDF4>)
- 612 • numpy (<http://www.numpy.org/>)
- 613 • scipy (<https://www.scipy.org/>)
- 614 • matplotlib (<https://matplotlib.org/>)
- 615 • matplotlib toolkit basemap (<https://matplotlib.org/basemap/>)

616 ATAT can be run from any Python enabled environment (e.g. IDLE, BASH). Here we provide the following
617 simple instructions for running ATAT in a BASH shell. For numerous runs, a shell script should be created.
618 From the command line, launch the ATAT script using python (“python ATATv1.1.py”). Eight command-line
619 arguments (A1 - A8), separated by a space should then follow.
620 A1 dictates whether deglacial or advance ages are being tested. Type “DEGLACIAL” or “ADVANCE”
621 accordingly.
622 A2 is the path to the geochronological data file (e.g. “/home/ATAT/geochron.nc”)
623 A3 defines whether the model extent is based on thickness or a mask. Type THK or MSK accordingly.
624 A4 is the path to the ice-sheet model output file (e.g. “/home/ATAT/icesheetmodel1.nc”)
625 A5 is the value of the ice-sheet output mask. A value is required even if A3 = THK, but can be any value as it will
626 be ignored.
627 A6 to A8 control output maps. A6 defines whether the output map should consider margin uncertainty, with a
628 value of BORDER or NONE.
629 A7 defines whether the model-data offset map displaces RMSE (option “NONE”) or wRMSE (“WEIGHTED”).
630 A8 specifies which dates are plotted on the difference map, and can be “ALL” for all dates, “COVERED” for
631 those which at some point were covered by ice and “INERROR” to display only those dates where model-data
632 agreement within dating error occurred.
633 An example command would be “python ATATv1.1.py DEGLACIAL /home/ATAT/dated_recon.nc MSK
634 /home/ATAT/experiment1.nc 2 BORDER WEIGHTED INERROR”. ATAT then outputs the two maps and a csv
635 table containing all derived statistics.
636 Input geochronological data can be created in a GIS environment such as ArcMap or QGIS. Here, the user must
637 discern the appropriate geochronological data for each grid cell. Since geochronological data is usually stored as
638 point data, this must be gridded to single grid points as positive values, with surrounding areas of no data assigned
639 a value of 0. When comparing to a reconstruction (e.g. Hughes et al., 2016), cells outside the reconstruction
640 should be assigned a value of 0. Those within the reconstruction should be assigned a value corresponding to the
641 reconstructed age of retreat. The gridded data must be converted to NetCDF format, the details of which are shown
642 in Table 3. We emphasise that the quality of geochronological data used must be considered, and an example of
643 how to filter geochronological data is documented in Small et al. (2017). Ice thickness grids can be created using
644 ice sheet modelling software such as PISM (Winkelmann et al., 2011). The two grids (data and model) must be
645 aligned and have the same size dimensions for use in ATAT. Examples are included as supplementary material,
646 including a model output from Ely et al. (in review).

647 *Acknowledgements:* This work was supported by the Natural Environment Research Council consortium grant;
648 BRITICE-CHRONO NE/J009768/1. Development of PISM is supported by NASA grant NNX17AG65G and

649 NSF grants PLR-1603799 and PLR-1644277. We thank Evan Gowan and Lev Tarasov for their constructive
650 reviews which improved the manuscript.

651 **References**

- 652 Auriac, A., Whitehouse, P.L., Bentley, M.J., Patton, H., Lloyd, J.M. and Hubbard, A. Glacial isostatic adjustment
653 associated with the Barents Sea ice sheet: a modelling inter-comparison. *Quaternary Science Reviews*, 147, 122-
654 135, 2016.
- 655 Applegate, P.J., Kirchner, N., Stone, E.J., Keller, K. and Greve, R. An assessment of key model parametric
656 uncertainties in projections of Greenland Ice Sheet behavior. *Cryosphere*, 6(3), 589-606, 2012.
- 657 Arnold, J.R. and Libby, W.F. Radiocarbon dates. *Science*, 113(2927), 111-120, 1951.
- 658 Balco, G. Contributions and unrealized potential contributions of cosmogenic-nuclide exposure dating to glacier
659 chronology, 1990–2010. *Quaternary Sci Rev*, 30(1), 3-27, 2011.
- 660 Bamber, J.L. and Aspinall, W.P.. An expert judgement assessment of future sea level rise from the ice sheets. *Nat*
661 *Clim Change*, 3(4), 424-427, 2013.
- 662 Bateman, M.D., Evans, D.J., Roberts, D.H., Medialdea, A., Ely, J. and Clark, C.D., The timing and consequences
663 of the blockage of the Humber Gap by the last British– Irish Ice Sheet. *Boreas*. 47(1), 41-61, 2018.
- 664 Boulton, G. and Hagdorn, M. Glaciology of the British Isles Ice Sheet during the last glacial cycle: form, flow,
665 streams and lobes. *Quaternary Sci Rev*, 25(23), 3359-3390, 2006.
- 666 Braconnot, P., Harrison, S.P., Kageyama, M., Bartlein, P.J., Masson-Delmotte, V., Abe-Ouchi, A., Otto-Bliesner,
667 B. and Zhao, Y., 2012. Evaluation of climate models using palaeoclimatic data. *Nature Climate Change*, 2(6),
668 417-424, 2012.
- 669 Briggs, R.D. and Tarasov, L. How to evaluate model-derived deglaciation chronologies: a case study using
670 Antarctica. *Quaternary Sci Rev*, 63, 109-127, 2013.
- 671 Briggs, R.D., Pollard, D. and Tarasov, L. A data-constrained large ensemble analysis of Antarctic evolution since
672 the Eemian. *Quaternary Sci Rev*, 103, 91-115, 2014.
- 673 Brown, E.J., Rose, J., Coope, R.G. and Lowe, J.J. An MIS 3 age organic deposit from Balglass Burn, central
674 Scotland: palaeoenvironmental significance and implications for the timing of the onset of the LGM ice sheet in
675 the vicinity of the British Isles. *J Quaternary Sci*, 22(3), 295-308, 2007.
- 676 Bueler, E.D., Lingle, C.S. and Brown, J. Fast computation of a viscoelastic deformable Earth model for ice-sheet
677 simulations. *Ann Glaciol*, 46(1), 97-105, 2007.
- 678 Bueler, E. and Brown, J. Shallow shelf approximation as a “sliding law” in a thermomechanically coupled ice
679 sheet model. *J Geophys Res-Earth*, 114(F3), 2009.
- 680 Calov, R. and Greve, R. A semi-analytical solution for the positive degree-day model with stochastic temperature
681 variations. *J Glaciol*, 51(172), 173-175, 2005.
- 682 Chiverrell, R.C., Thrasher, I.M., Thomas, G.S., Lang, A., Scourse, J.D., van Landeghem, K.J., Mccarroll, D.,
683 Clark, C.D., Cofaigh, C.Ó., Evans, D.J. and Ballantyne, C.K. Bayesian modelling the retreat of the Irish Sea Ice
684 Stream. *J Quaternary Sci*, 28(2), 200-209, 2013.
- 685 Clark, C.D., Hughes, A.L., Greenwood, S.L., Jordan, C. and Sejrup, H.P. Pattern and timing of retreat of the last
686 British-Irish Ice Sheet. *Quaternary Sci Rev*, 44, 112-146, 2012.

687 [Collins, M. Ensembles and probabilities: a new era in the prediction of climate change. *Philos T R Soc A*, 365,](#)
688 [1857, 2007.](#)

689 [Collins, M., Booth, B.B., Bhaskaran, B., Harris, G.R., Murphy, J.M., Sexton, D.M. and Webb, M.J. Climate model](#)
690 [errors, feedbacks and forcings: a comparison of perturbed physics and multi-model ensembles. *Clim*](#)
691 [Dynam.](#) 36(9-10), 1737-1766, 2011.

692 Cornford, S.L., Martin, D.F., Graves, D.T., Ranken, D.F., Le Brocq, A.M., Gladstone, R.M., Payne, A.J., Ng,
693 E.G. and Lipscomb, W.H. Adaptive mesh, finite volume modeling of marine ice sheets. *Journal of Computational*
694 *Physics*, 232(1), 529-549, 2013.

695 DeConto, R.M. and Pollard, D. Contribution of Antarctica to past and future sea-level rise. *Nature*, 531(7596),
696 591-597, 2016.

697 Duller, G.A.T. Single grain optical dating of glacial deposits. *Quaternary Geochronology*, 1(4), 296-304, 2006.

698 Dyke, A.S. An outline of North American deglaciation with emphasis on central and northern Canada.
699 *Developments in Quaternary Sciences*, 2, 373-424, 2004.

700 Dyke, A.S. An outline of North American deglaciation with emphasis on central and northern Canada.
701 *Developments in Quaternary Sciences*, 2, 373-424, 2004.

702 Edwards, T.L., Fettweis, X., Gagliardini, O., Gillet-Chaulet, F., Goelzer, H., Gregory, J.M., Hoffman, M.,
703 Huybrechts, P., Payne, A.J., Perego, M. and Price, S. Effect of uncertainty in surface mass balance-elevation
704 feedback on projections of the future sea level contribution of the Greenland ice sheet. *Cryosphere*, 8(1), 195-208.
705 2014.

706 Ely, J.C., Clark, C.D., Hindmarsh, R.C.A., Hughes, A.L.C., Greenwood, S.L., Bradley, S.L., Gasson, E., Gregoire,
707 L., Gandy, N., Stokes, C.R. and Small, D. An approach to combining geomorphological and geochronological
708 data with ice sheet modelling, demonstrated using the last British-Irish Ice Sheet. *Journal of Quaternary Science*.
709 In review.

710 Fowler, A.C. A sliding law for glaciers of constant viscosity in the presence of subglacial cavitation. In
711 *Proceedings of the Royal Society of London A: Mathematical, Physical and Engineering Sciences*, 407(1832),
712 147-170, 1986.

713 Fretwell, P., Pritchard, H.D., Vaughan, D., Bamber, J.L., Barrand, N.E., Bell, R., Bianchi, C., Bingham, R.G.,
714 Blankenship, D.D., Casassa, G. and Catania, G. Bedmap2: improved ice bed, surface and thickness datasets for
715 Antarctica. *Cryosphere*, 7, 375-393, 2013.

716 Fuchs, M. and Owen, L.A. Luminescence dating of glacial and associated sediments: review, recommendations
717 and future directions. *Boreas*, 37(4), 636-659, 2008.

718 Gasson, E., DeConto, R.M., Pollard, D. and Levy, R.H. Dynamic Antarctic ice sheet during the early to mid-
719 Miocene. *Proceedings of the National Academy of Sciences*, 113(13), 3459-3464, 2016.

720 Golledge, N.R., Levy, R.H., McKay, R.M., Fogwill, C.J., White, D.A., Graham, A.G., Smith, J.A., Hillenbrand,
721 C.D., Licht, K.J., Denton, G.H. and Ackert, R.P. Glaciology and geological signature of the Last Glacial
722 Maximum Antarctic ice sheet. *Quaternary Sci Rev*, 78, 225-247, 2013.

723 Gomez, N., Pollard, D., Mitrovica, J.X., Huybers, P., Clark, P.U. Evolution of a coupled marine ice sheet-sea
724 level model, *J Geophys Res*, 117, F01013, 2012.

725 Gomez, N., Pollard, D. and Mitrovica, J.X. A 3-D coupled ice sheet-sea level model applied to Antarctica through
726 the last 40 ky. *Earth and Planet Sc Lett*, 384, 88-99, 2013.

Formatted: Font: Not Italic

727 Gowan, E.J. An assessment of the minimum timing of ice free conditions of the western Laurentide Ice Sheet.
728 *Quaternary Sci Rev*, 75, 100-113, 2013.

729 Gregoire, L.J., Payne, A.J. and Valdes, P.J. Deglacial rapid sea level rises caused by ice-sheet saddle collapses.
730 *Nature*, 487(7406), 219-222, 2012.

731 Greve, R. and Hutter, K. Polythermal three-dimensional modelling of the Greenland ice sheet with varied
732 geothermal heat flux. *Ann. Glaciol.*, 21, 8-12, 1995.

733 Greve, R., Wyrwoll, K.H. and Eisenhauer, A. Deglaciation of the Northern Hemisphere at the onset of the Eemian
734 and Holocene. *Ann. Glaciol.*, 28, 1-8, 1999.

735 Gudmundsson, G.H., Krug, J., Durand, G., Favier, L. and Gagliardini, O. The stability of grounding lines on
736 retrograde slopes. *Cryosphere*, 6, 1497-1505, 2012.

737 Gudmundsson, G.H. Ice-shelf buttressing and the stability of marine ice sheets, *Cryosphere*, 7, 647-655, 2013.

738 Heroy, D.C. and Anderson, J.B. Radiocarbon constraints on Antarctic Peninsula ice sheet retreat following the
739 Last Glacial Maximum (LGM). *Quaternary Sci Rev*, 26(25), 3286-3297, 2007.

740 Heyman, J., Stroeven, A.P., Harbor, J.M. and Caffee, M.W. Too young or too old: evaluating cosmogenic
741 exposure dating based on an analysis of compiled boulder exposure ages. *Earth Planet Sc Lett*, 302(1), 71-80,
742 2011.

743 Hindmarsh, R.C. Consistent generation of ice-streams via thermo-viscous instabilities modulated by membrane
744 stresses. *Geophys Res Lett*, 36(6). 2009.

745 Hubbard, A., Bradwell, T., Gollledge, N., Hall, A., Patton, H., Sugden, D., Cooper, R. and Stoker, M. Dynamic
746 cycles, ice streams and their impact on the extent, chronology and deglaciation of the British-Irish ice sheet.
747 *Quaternary Sci Rev*, 28(7), 758-776, 2009.

748 Hughes, A.L., Greenwood, S.L. and Clark, C.D. Dating constraints on the last British-Irish Ice Sheet: a map and
749 database. *J Maps*, 7(1), 156-184, 2011.

750 Hughes, A.L., Clark, C.D. and Jordan, C.J. Flow-pattern evolution of the last British Ice Sheet. *Quaternary Sci*
751 *Rev*, 89, 148-168, 2014.

752 Hughes, A.L., Gyllencreutz, R., Lohne, Ø.S., Mangerud, J. and Svendsen, J.I. The last Eurasian ice sheets—a
753 chronological database and time-slice reconstruction, DATED-1. *Boreas*, 45(1), 1-45, 2016.

754 Hughes, T.J., Is the West Antarctic ice sheet disintegrating? *J. Geophys. Res.*, 78 (33), 7884-7910, 1973.

755 Huybrechts, P. The Antarctic ice sheet during the last glacial-interglacial cycle: a three-dimensional
756 experiment. *Ann. Glaciol.* 14, 115-119, 1990.

757 Imbrie, J., Hays, J.D., Martinson, D.G., McIntyre, A., Mix, A.C., Morley, J.J., Pisias, N.G., Prell, W.L.,
758 Shackleton, N.J. The orbital theory of Pleistocene climate: support from a revised chronology of the marine $\delta^{18}O$
759 record. In: Berger, A., Imbrie, J., Hays, H., Kukla, G., Saltzman, B. (Eds.), *Milankovitch and Climate, Part I*. D.
760 Reidel Publishing, Dordrecht, 269–305, 1984.

761 Johnsen, S.J., Dahl-Jensen, D., Dansgaard, W. and Gundestrup, N. Greenland palaeotemperatures derived from
762 GRIP bore hole temperature and ice core isotope profiles. *Tellus B*, 47(5), 624-629, 1995.

763 Kirchner, N., Hutter, K., Jakobsson, M. and Gyllencreutz, R. Capabilities and limitations of numerical ice sheet
764 models: a discussion for Earth-scientists and modelers. *Quaternary Sci Rev*, 30(25), 3691-3704, 2011.

765 Kirchner, N., Ahlkrona, J., Gowan, E.J., Lötstedt, P., Lea, J.M., Noormets, R., von Sydow, L., Dowdeswell, J.A.
766 and Benham, T. Shallow ice approximation, second order shallow ice approximation, and full Stokes models: A
767 discussion of their roles in palaeo-ice sheet modelling and development. *Quaternary Sci Rev*, 147, 136-147, 2016.
768 Kleman, J., Hättestrand, C., Stroeven, A.P., Jansson, K.N., De Angelis, H. and Borgström, I. Reconstruction of
769 Palaeo-Ice Sheets-Inversion of their Glacial Geomorphological Record. In Knight, P.G. (Eds) *Glacier science and
770 environmental change*, 192-198, 2006.
771 Larour, E., Seroussi, H., Morlighem, M. and Rignot, E. Continental scale, high order, high spatial resolution, ice
772 sheet modeling using the Ice Sheet System Model (ISSM). *J Geophys Res-Earth*, 117(F1), 2012.
773 Libby, W.F., Anderson, E.C. and Arnold, J.R. Age determination by radiocarbon content: world-wide assay of
774 natural radiocarbon. *Science*, 109(2827), 227-228, 1949.
775 Lingle, C.S. and Clark, J.A. A numerical model of interactions between a marine ice sheet and the solid earth:
776 Application to a West Antarctic ice stream. *J Geophys Res-Oceans*, 90(C1), 1100-1114, 1985.
777 Livingstone, S.J., Cofaigh, C.Ó., Stokes, C.R., Hillenbrand, C.D., Vieli, A. and Jamieson, S.S. Antarctic palaeo-
778 ice streams. *Earth-Sci Rev*, 111(1), 90-128, 2012.
779 Lorenz, E.N. Deterministic Nonperiodic Flow, *J. Atmos. Sci.*, 20, 130-141, 1963.
780 Lowe, J.J. and Walker, M.J. Radiocarbon Dating the Last Glacial-Interglacial Transition (Ca. 14–9 14C Ka Bp)
781 in Terrestrial and Marine Records: The Need for New Quality Assurance Protocols. *Radiocarbon*, 42(1), 53-68,
782 2000.
783 Lowell, T.V., Fisher, T.G., Hajdas, I., Glover, K., Loope, H. and Henry, T. Radiocarbon deglaciation chronology
784 of the Thunder Bay, Ontario area and implications for ice sheet retreat patterns. *Quaternary Sci Rev*, 28(17), 1597-
785 1607, 2009.
786 Lukas, S., Spencer, J.Q., Robinson, R.A. and Benn, D.I. Problems associated with luminescence dating of Late
787 Quaternary glacial sediments in the NW Scottish Highlands. *Quaternary Geochron*, 2(1), 243-248, 2007.
788 Mercer, J.H. West Antarctic ice sheet and CO₂ greenhouse effect: a threat of disaster. *Nature*, 271, 321-325, 1978.
789 Napieralski, J., Harbor, J. and Li, Y. Glacial geomorphology and geographic information systems. *Earth-Sci Rev*,
790 85(1), 1-22, 2007.
791 [Murphy, J.M., Sexton, D.M., Barnett, D.N., Jones, G.S., Webb, M.J., Collins, M. and Stainforth, D.A.](#)
792 [Quantification of modelling uncertainties in a large ensemble of climate change simulations. *Nature*, 430\(7001\),](#)
793 [768-771. 2004.](#)
794 Ó Cofaigh, C.Ó. and Evans, D.J. Radiocarbon constraints on the age of the maximum advance of the British-Irish
795 Ice Sheet in the Celtic Sea. *Quaternary Sci Rev*, 26(9), 1197-1203, 2007.
796 Patton, H., Hubbard, A., Andreassen, K., Winsborrow, M. and Stroeven, A.P. The build-up, configuration, and
797 dynamical sensitivity of the Eurasian ice-sheet complex to Late Weichselian climatic and oceanic forcing.
798 *Quaternary Sci Rev*, 153, 97-121, 2016.
799 Pattyn, F. Sea-level response to melting of Antarctic ice shelves on multi-centennial timescales with the fast
800 Elementary Thermomechanical Ice Sheet model (f. ETISH v1. 0). *Cryosphere*, 11(4), p.1851-1878, 2017.
801 Pattyn, F., Perichon, L., Aschwanden, A., Breuer, B., De Smedt, B., Gagliardini, O., Gudmundsson, G.H.,
802 Hindmarsh, R., Hubbard, A., Johnson, J.V. and Kleiner, T. Benchmark experiments for higher-order and full
803 Stokes ice sheet models (ISMIP-HOM). *Cryosphere*, 2(1), 111-151, 2008.

Formatted: Font: Not Italic

Formatted: Font: Not Italic

804 Pattyn, F., Schoof, C., Perichon, L., Hindmarsh, R.C.A., Bueller, E., Fleurian, B.D., Durand, G., Gagliardini, O.,
805 Gladstone, R., Goldberg, D. and Gudmundsson, G.H. Results of the marine ice sheet model intercomparison
806 project, MISMIP. *Cryosphere*, 6(3), 573-588, 2012.

807 Pollard, D. and DeConto, R.M. Modelling West Antarctic ice sheet growth and collapse through the past five
808 million years. *Nature*, 458(7236), 329-332, 2009.

809 Ritz, C., Edwards, T.L., Durand, G., Payne, A.J., Peyaud, V. and Hindmarsh, R.C. Potential sea-level rise from
810 Antarctic ice-sheet instability constrained by observations. *Nature*, 528(7580), 115-118, 2015.

811 Robinson, A., Calov, R. and Ganopolski, A. Greenland ice sheet model parameters constrained using simulations
812 of the Eemian Interglacial. *Clim Past*, 7(2), 381-396, 2011.

813 Rougier, J., 2007. Probabilistic inference for future climate using an ensemble of climate model
814 evaluations. *Climatic Change*, 81(3-4), pp.247-264.

815 Rutt, I.C., Hagdorn, M., Hulton, N.R.J. and Payne, A.J. The Glimmer community ice sheet model. *J. Geophys.*
816 *Res-Earth*, 114(F2), 2009.

817 Schoof, C.S. Ice sheet grounding line dynamics: steady states, stability and hysteresis. *J. Geophys. Res. Earth*
818 *Surf.*, 112, F03S28, 2007.

819 Schoof, C. Coulomb friction and other sliding laws in a higher-order glacier flow model. *Math Mod Meth Appl*
820 *S*, 20(01), 157-189, 2010.

821 Schoof, C. Marine ice sheet stability. *J. Fluid Mech.*, 698, 62-72, 2012.

822 Seddik, H., Greve, R., Zwinger, T., Gillet-Chaulet, F. and Gagliardini, O. Simulations of the Greenland ice sheet
823 100 years into the future with the full Stokes model Elmer/Ice. *J Glaciol*, 58(209), 427-440, 2012.

824 Seguinot, J., Rogozhina, I., Stroeve, A.P., Margold, M. and Kleman, J. Numerical simulations of the Cordilleran
825 ice sheet through the last glacial cycle. *Cryosphere*, 10, 639-664, 2016.

826 Simpson, M.J., Milne, G.A., Huybrechts, P. and Long, A.J. Calibrating a glaciological model of the Greenland
827 ice sheet from the Last Glacial Maximum to present-day using field observations of relative sea level and ice
828 extent. *Quaternary Sci Rev*, 28(17), 1631-1657, 2009.

829 Small, D., Clark, C.D., Chiverrell, R.C., Smedley, R.K., Bateman, M.D., Duller, G.A., Ely, J.C., Fabel, D.,
830 Medialdea, A. and Moreton, S.G. Devising quality assurance procedures for assessment of legacy
831 geochronological data relating to deglaciation of the last British-Irish Ice Sheet. *Earth-Sci Rev*, 164, 232-250,
832 2017.

833 Smedley, R.K., Glasser, N.F. and Duller, G.A.T. Luminescence dating of glacial advances at Lago Buenos Aires
834 (~ 46° S), Patagonia. *Quaternary Sci Rev*, 134, 59-73, 2016.

835 Smedley, R.K., Chiverrell, R.C., Ballantyne, C.K., Burke, M.J., Clark, C.D., Duller, G.A.T., Fabel, D., McCarroll,
836 D., Scourse, J.D., Small, D. and Thomas, G.S.P. Internal dynamics condition centennial-scale oscillations in
837 marine-based ice-stream retreat. *Geology*, 45(9), 787-790, 2017.

838 Stokes, C.R., Tarasov, L., Blomdin, R., Cronin, T.M., Fisher, T.G., Gyllencreutz, R., Hättestrand, C., Heyman, J.,
839 Hindmarsh, R.C., Hughes, A.L. and Jakobsson, M. On the reconstruction of palaeo-ice sheets: recent advances
840 and future challenges. *Quaternary Sci Rev*, 125, 15-49, 2015.

841 Tarasov, L. and Peltier, W.R. A geophysically constrained large ensemble analysis of the deglacial history of the
842 North American ice-sheet complex. *Quaternary Sci Rev*, 23(3), 359-388, 2004.

843 Tarasov, L., Dyke, A.S., Neal, R.M. and Peltier, W.R. A data-calibrated distribution of deglacial chronologies for
 844 the North American ice complex from glaciological modeling. *Earth Planet Sc Lett*, 315, 30-40, 2012.

845 [Tebaldi, C. and Knutti, R. The use of the multi-model ensemble in probabilistic climate projections. *Philos T R*
 846 *Soc A*, 365\(1857\), 2053-2075, 2007.](#)

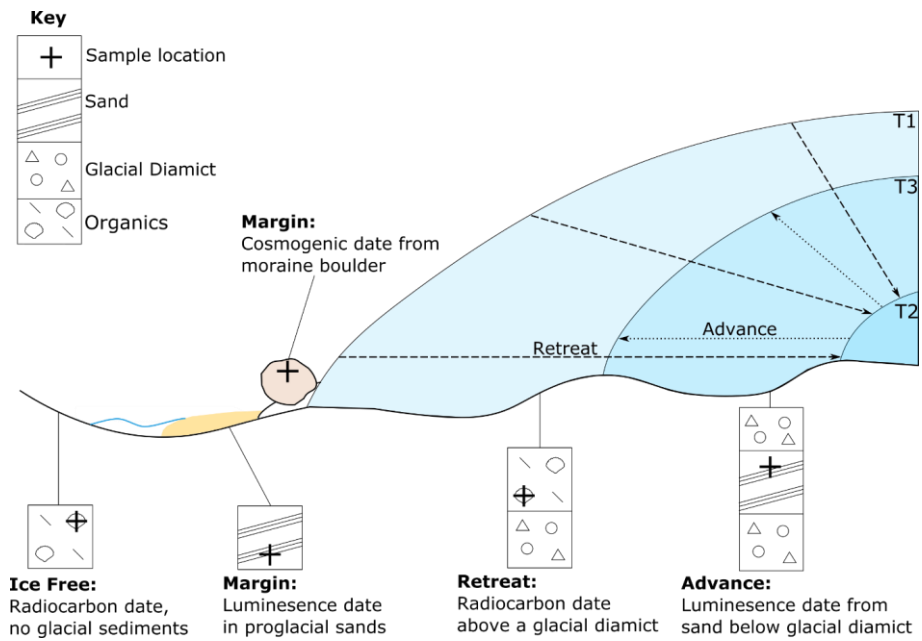
847 Tushingham, A.M. and Peltier, W.R. Validation of the ICE-3G Model of Würm-Wisconsin Deglaciation using a
 848 global data base of relative sea level histories. *J Geophys Res-Solid Earth*, 97(B3), 3285-3304, 1992.

849 Weertman, J. Stability of the junction of an ice-sheet and an ice-shelf. *J. Glaciol.* 13 (67), 3-11, 1974.

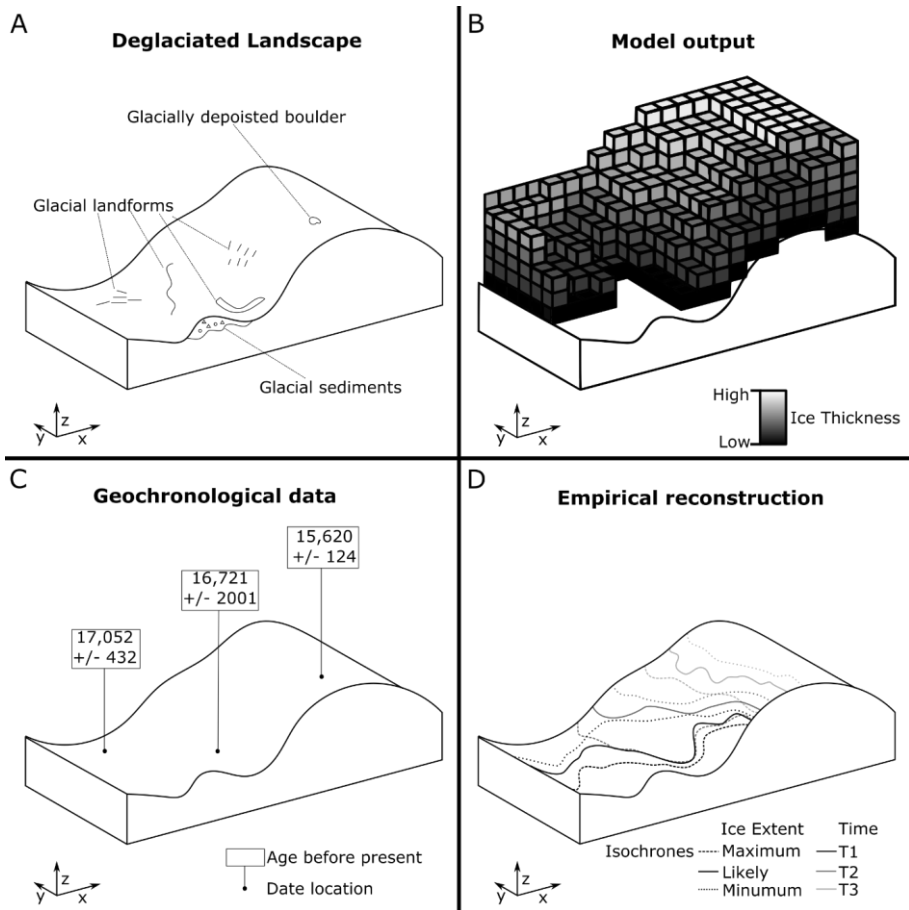
850 Winkelmann, R., Martin, M.A., Haseloff, M., Albrecht, T., Bueler, E., Khroulev, C. and Levermann, A. The
 851 Potsdam parallel ice sheet model (PISM-PIK)-Part 1: Model description. *Cryosphere*, 5(3), 715-726, 2011.

852
853
854
855
856
857
858

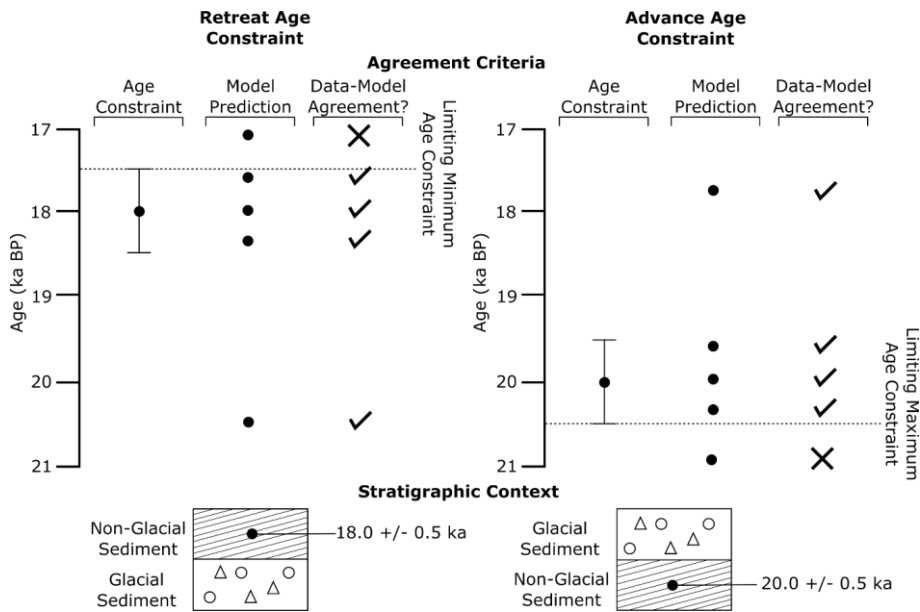
Formatted: Font: Not Italic



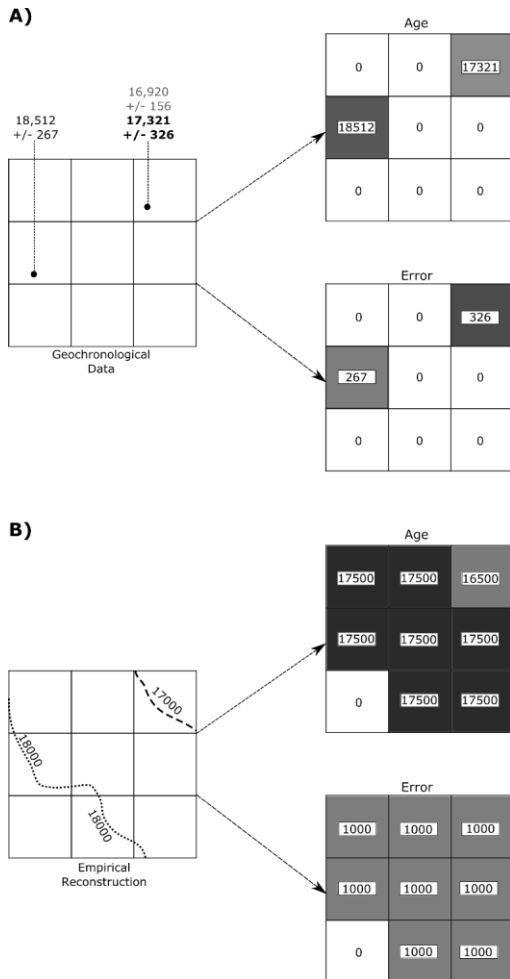
859
860 **Figure 1: Schematic illustration of stratigraphic and inferred glaciological context of geochronological data. Note that**
 861 **at T1 the ice sheet is at its most advanced. It then retreats to a minimum at T2, before re-advancing to T3.**



862
 863 **Figure 2. Schematic of geochronological data and ice-sheet model output.** A) A deglaciaded landscape,
 864 demonstrating some of the features used by palaeo-glaciologists when empirically reconstructing an ice
 865 sheet. B) Ice-sheet model output, displaying modelled ice-sheet thickness, in this case at a specific time. C)
 866 Geochronological data. D) Empirical reconstruction. Note how the nature of these data vary between
 867 source.

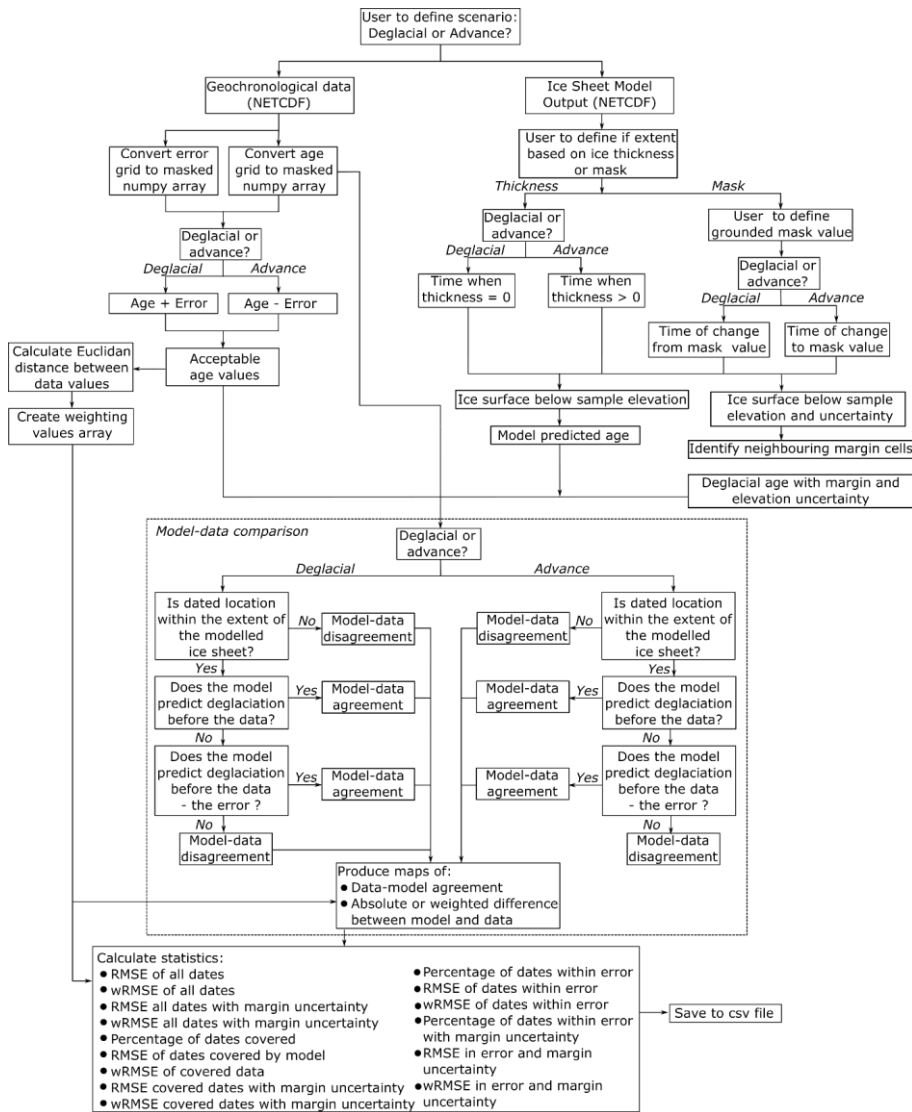


868
 869 **Figure 3. Schematic of the identification of data-model agreement with consideration of error by ATAT for**
 870 **retreat (left) and advance (right) data. If a model predicts ice free conditions before an ice-free age, or**
 871 **during the associated error, there is data-model agreement. If deglaciation occurs at this location after the**
 872 **error, the model disagrees with the data. If a model predicts ice advance and cover before the advance age**
 873 **and its associated error, there is model-data disagreement. Agreement between the model and data occurs**
 874 **if ice advances over the location after the date, or before the date within the range of the error. This is used**
 875 **by ATAT to categorise sites as to whether agreement or disagreement between the model and data occurs.**



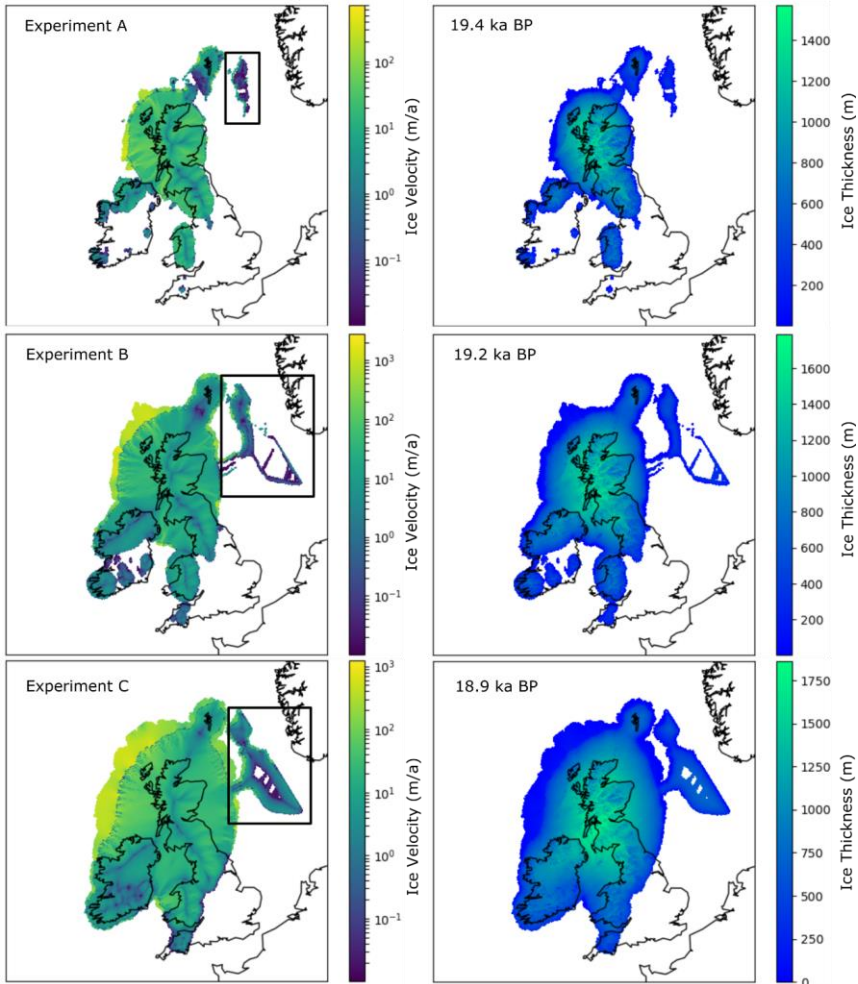
876

877 **Figure 4. Examples of empirical data preparation for ATAT. (A) Conversion of geochronological data into**
 878 **a grid for ATAT. In this example the user has made a judgement based on a priori knowledge that the date**
 879 **of 17,321 ± 326 is most representative of the event of interest. Note that age and error are split into separate**
 880 **grids, and that no data regions are assigned a value of 0. (B) Conversion of an empirical reconstruction**
 881 **(margin isochrones) into a grid for ATAT. Here we simply assume that the area between isochrones became**
 882 **deglaciated between at the age between the two isochrones, and that associated error is 1000 years. More**
 883 **complex reconstructions (e.g. Hughes et al., 2016) may require different user-defined rules.**

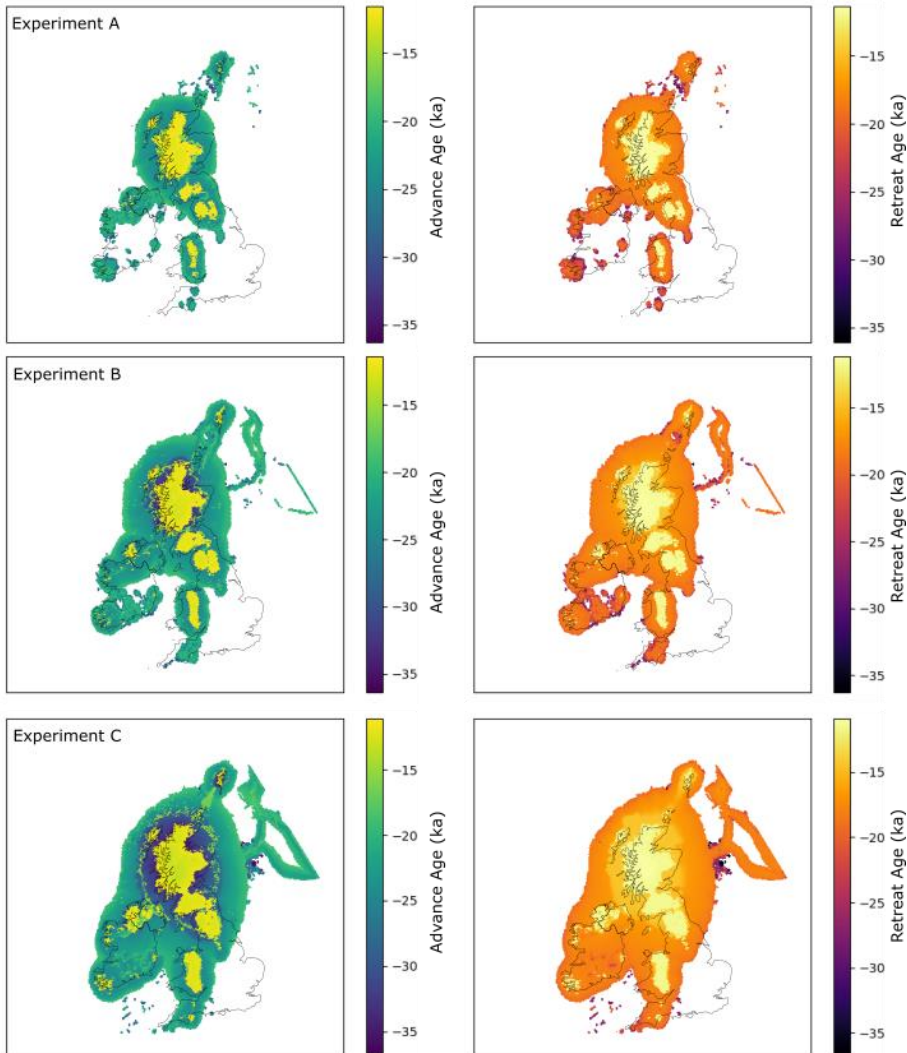


884

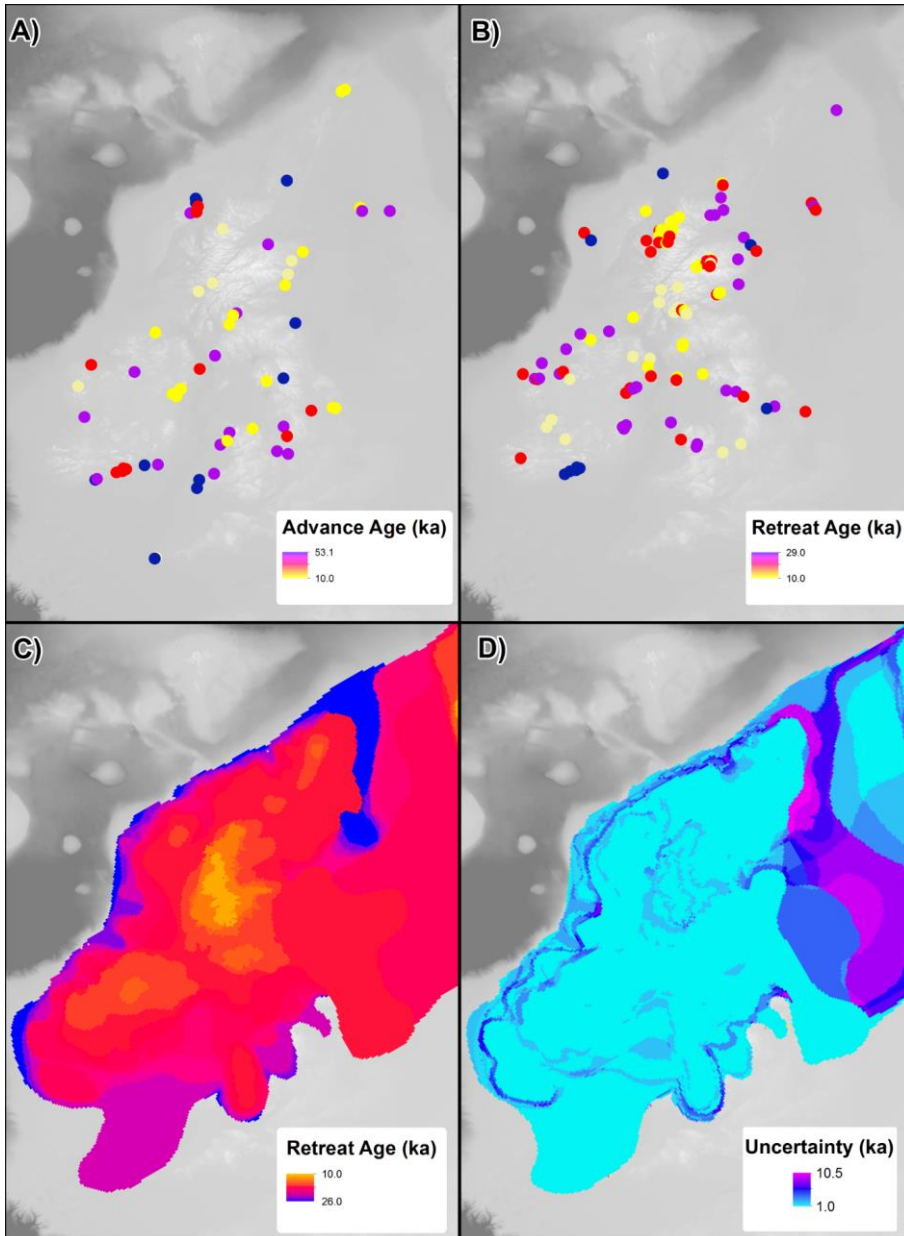
885 **Figure 5. Flow chart of ATAT procedure. See text for further description.**



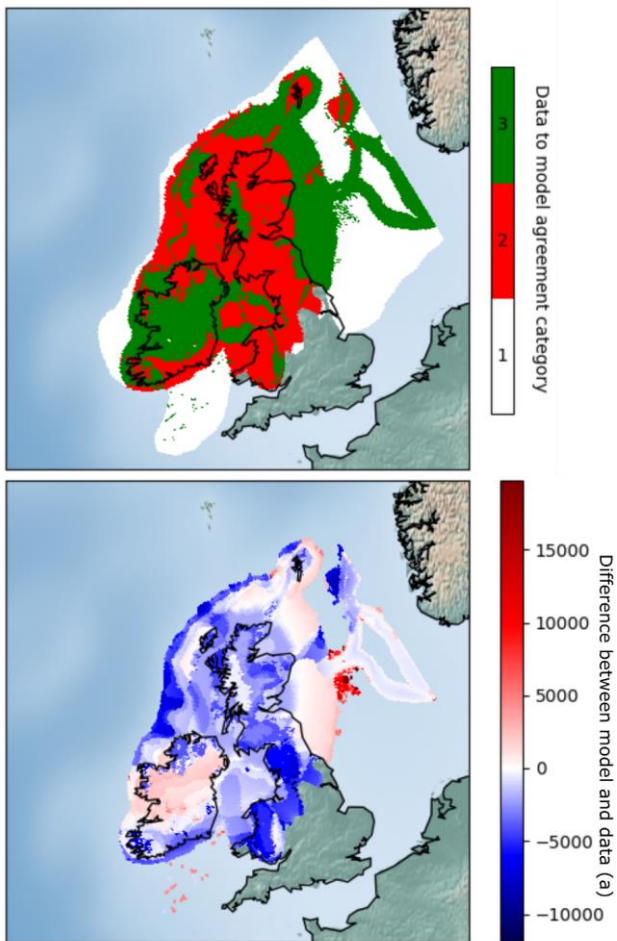
886
 887 **Figure 6. Maximum extent of produced ice sheet for the three experiments. Experiment B is 1°C colder**
 888 **than A, and experiment C is 2°C colder than A. Left panel shows ice velocity, right is ice thickness. The box**
 889 **on the left panel highlights likely erroneous output in the North Sea, likely a consequence of model domain,**
 890 **discussed further in the text.**



891
 892 **Figure 7. Timing of advance (left) and retreat (right) from the three ice sheet modelling experiments.**
 893 **Experiments are the same as in Figure 6. The early ages toward the centre of the model, and centred over**
 894 **higher topography, represent the modelled extent of the Younger Dryas readvance.**



895
 896 **Figure 8.** Example of geochronological data projected onto model raster grids; as point-data in A and B
 897 and from an empirical reconstruction in C and D. (A). Advance ages from Hughes et al. (2016). (B) Retreat
 898 ages from Small et al. (2017). (C) Retreat age derived from DATED isochrone reconstruction (Hughes et
 899 al., 2016). (D) Error associated with reconstruction in C.



900
 901 **Figure 9.** Example mapped outputs from ATAT. In this case, experiment C was compared with the DATED
 902 reconstruction. Top map (cumulative agreement) shows categories of data-model agreement across the
 903 domain, where 1 = not covered by model, 2 = no agreement and 3 = data-model agreement within error.
 904 The lower map (model-data offset) shows magnitude of difference between model and data; negative values
 905 show a modelled retreat of ice later than the DATED isochrones, and positive values show a modelled
 906 retreat of ice before the DATED isochrones.

907 Table 1. Classification of geochronological data (after Hughes et al., 2011) and its use in ATAT.

Class	Glaciological context	Stratigraphic context	Example	Use in ATAT
Advance	Ice-sheet build up	Material directly below or incorporated within glacial diamict	Luminescence date from a sand below a glacial diamict	Ice cover a short time after this date
Retreat	Ice-free after ice cover	Dated material above glacial diamict	Radiocarbon date of a shell above a glacial diamict	Ice-free conditions from this date onwards (note deglaciation could have occurred a long time before)
Ice Free	Ice-free, but lacking direct information regarding ice	Dated material which indicates ice-free conditions but has no relation to ice cover. It may be much younger and not provide much useful constraint.	Radiocarbon date of organic sediments without underlying glacial sediments	
Margin	Proximal to an ice sheet margin	Dated material with information that ties it to an ice margin	Luminescence date in proglacial sands	
Exposure time (cumulative)	Length of time since sample exposed	N/A	Cosmogenic isotope on erratic boulder above a trimline	Not used

908

Table 2. Comparison of attributes between geochronological data and ice sheet model output.

	Nature of data produced	Spatial resolution	Spatial continuity	Temporal frequency and resolution	Sources of uncertainty	Main limitation
Geochronological data	Timing of the absence of ice at a location	Point location	Point location, unevenly distributed in space, but can be interpolated	Determined by data availability and associated error	Instrumental, environmental and stratigraphic factors	Reliant upon correct stratigraphic interpretation to tie to glaciological events
Ice-sheet model output	Simulation of physically plausible ice sheet conditions	Various, ranging from tens to unit kilometres.	Spatially even, regularly-spaced across entire domain	Continuous in time. Precise subannual resolution possible, but not recorded in practice	Parameterisations, boundary conditions	Based upon mathematical and physical approximations of ice flow

Data source	NetCDF Variable	Units	Dimensions	Description	Notes
	Time	Time unit	x, y	Calendar years before present	
Ice sheet model output		before reference calendar date			
	thk	m	time, x,y	Ice thickness	Either “thk” or “msk” required by ATAT.
	msk	Integers	time, x,y	Grounded/floating/icefree mask	Either “thk” or “msk” required by ATAT. User defines value referring to the location of grounded ice
Both	lat	Decimal degrees	x, y	Latitude	
	lon	Decimal degrees	x, y	Longitude	
Geochronological data	age	Time unit	x, y	Timing of deglaciaded conditions	Deglacial and advance ages must be in separate files.
		before reference calendar date			
	error	Seconds	x, y	Error associated with deglaciaded conditions	Error associated with either deglacial and advance age must be in associated separate file.
	topg	m	x,y	Modern elevation at resolution of ice-sheet model	

elevation m x,y Elevation of collected sample

Table 3. Required input variables for ATAT NetCDF files.

Table 4: Example statistics from ATAT. Note that the RMSE is often altered by applying the spatial weighting to create wRMSE.

	Advance			Retreat			Empirical Reconstruction; DATED		
Ice Sheet Modelling Experiment	A	B	C	A	B	C	A	B	C
Percentage of dates covered	52.5	72.1	88.5	76.1	91.7	96.3	32.9	52.6	69.8
Percentage that agree within error	65.6	72.7	72.2	22.0	22.0	12.8	23.2	27.0	17.8
RMSE dates covered by model	11075.9	12732.7	13490.3	3879.0	4180.9	4945.4	2972.5	2678.0	2920.8
wRMSE dates covered by model	13357.3	13994.7	14849.7	4073.4	4450.3	5165.8	N/A	N/A	N/A
RMSE dates within error	655.7	478.6	289.3	403.6	259.7	236.2	12023.4	10638.7	8777.6
wRMSE dates within error	615.4	395.0	223.6	422.1	276.9	248.9	N/A	N/A	N/A